

Photometry of the Stingray Nebula (V839 Ara) from 1889-2015 Across the Ionization of Its Planetary Nebula

Bradley E. Schaefer & Zachary I. Edwards

Physics and Astronomy, Louisiana State University, Baton Rouge, LA 70803

ABSTRACT

Up until around 1980, the Stingray was an ordinary B1 post-AGB star, but then it suddenly sprouted bright emission lines like in a planetary nebula (PN), and soon after this the *Hubble Space Telescope (HST)* discovered a small PN around the star, so apparently we have caught a star in the act of ionizing a PN. We report here on a well-sampled light curve from 1889 to 2015, with unique coverage of the prior century plus the entire duration of the PN formation plus three decades of its aftermath. Surprisingly, the star anticipated the 1980's ionization event by declining from $B=10.30$ in 1889 to $B=10.76$ in 1980. Starting in 1980, the central star faded fast, at a rate of 0.20 mag/year, reaching $B=14.64$ in 1996. This fast fading is apparently caused by the central star shrinking in size. From 1994-2015, the V-band light curve is almost entirely from the flux of two bright [OIII] emission lines from the unresolved nebula, and it shows a consistent decline at a rate of 0.090 mag/year. This steady fading (also seen in the radio and infrared) has a time scale equal to that expected for ordinary recombination within the nebula, immediately after a short-duration ionizing event in the 1980s. We are providing the first direct measure of the rapidly changing luminosity of the central star on both sides of a presumed thermal pulse in 1980, with this providing a strong and critical set of constraints, and these are found to sharply disagree with theoretical models of PN evolution.

Subject headings: stars: AGB and post-AGB — planetary nebulae: general — planetary nebulae: individual (Stingray Nebula) — stars: individual (V839 Ara)

1. Background

The ‘Stingray Nebula’ (V839 Ara, SAO 244567, CD $-59^{\circ} 6479$, CPD $-59^{\circ} 6926$, Hen 3-1357, and PN G331-12.1) is a unique case where an ordinary post asymptotic giant branch (post-AGB) star suddenly changed its appearance to that of a young planetary nebula (PN). This ejection of the PN shell was roughly one millennium ago, but the nebula turned on

suddenly around 1980 with some sharp increase in ionizing radiation. The Stingray represents our one opportunity to actually watch the turn-on of a PN.

Before 1980, four spectra of the Stingray have been published, all showing either very weak Balmer emission lines or no emission lines (see the timeline in Table 1). During this time, as best seen in the 1971 spectrum (Parthasarathy et al. 1995), the spectrum was that of a normal B0 or B1 star, placed into luminosity class I or II, with possible weak emission at $H\beta$ only. The star slowly began to attract attention, first for having just some $H\alpha$ emission (Henize 1976), then as an *IRAS* far-infrared source selected out as a proto-planetary nebula (Volk & Kwok 1989; Parthasarathy & Pottasch 1989), then as a star that had a sudden appearance of a PN shell within the previous few years (Parthasarathy et al. 1993). By 1990 and 1992, the Stingray optical spectrum was dominated by very bright and narrow [OIII] emission lines, plus other lines that are characteristic of a young PN (Parthasarathy et al. 1993; 1995). The stark difference between the 1971 spectrum (a B1I star with weak emission only) and the 1990 spectrum (very bright PN emission lines) impresses that the Stingray is evolving fast and apparently the PN has just turned-on.

From the start of the 1980’s event with the fast turn-on of the PN spectrum, the Stingray has been fast evolving (see Table 1). At the start, a B0 spectrum gives a surface temperature of around 30,000 K. From the time of the first *International Ultraviolet Explorer (IUE)* spectrum, the effective temperature of the star has been heating up greatly (Parthasarathy et al. 1995), going from 38,000 K in 1988 to 55,000 K in 2006 (Reindl et al. 2014). The surface gravity has increased from $10^{4.8}$ cm s^{-2} in 1988 to $10^{6.0}$ cm s^{-2} in 2006 (Reindl et al. 2014). The mass ejection rate has decreased from $10^{-9.0}$ M_{\odot} year^{-1} in 1988 to $10^{-11.6}$ M_{\odot} year^{-1} in 2006 (Reindl et al. 2014). The ultraviolet continuum brightness has fallen by a factor of three from 1988 to 1994 (Parthasarathy et al. 1995; Feibelman 1995), continued to fall by another factor of three to 1997, but then brightened by a factor of two in 2002 and 2006 (Reindl et al. 2014). We have a clear picture of a star in 1988 with a high stellar wind, that rapidly tapered off, while the star shrunk in size (by a factor of four) and heated up. The shrinking and heating of the central star is what would be expected for a simple picture of a stellar core following along the evolutionary track that leads to a white dwarf.

The first distance measure to the Stingray was 5.64 kpc (Kozok 1985b), based on a presumed absolute magnitude appropriate for the star’s color, and as such this estimate has a very large real uncertainty. Fresneau et al. (2007) measure the proper motion of the Stingray, and from this derive a statistical parallax of 1.21 ± 0.21 milli-arc-seconds (for a distance of 830 pc and an uncertainty of 17%), while the possible deviation from their statistical model makes for a possibly large error in this distance. The best distance to the Stingray is based on the luminosity calculated from the measured temperature and surface

gravity, with resulting distances of $1.6_{-1.2}^{+0.8}$ kpc (Reindl et al. 2014) and ≈ 1.8 kpc (Arkhipova et al. 2013). The interstellar extinction has $E(B - V)$ equal to 0.20 ± 0.05 mag (as based on the 2200\AA feature in the ultraviolet) and 0.14 mag (based on the observed Balmer decrement) (Parthasarathy et al. 1993). The measured extinction has not changed significantly from 1980 to 2011 (Reindl et al. 2014). The deduced mass for the star is variously given as $< 0.55 M_{\odot}$ (Reindl et al. 2014) or $0.2 + 0.59 M_{\odot}$ for the ionized mass plus the core mass (Bobrowsky 1994).

The expanding PN shell was resolved in 1992 by the *Hubble Space Telescope* (*HST*) to be bipolar shaped with an embedded ‘equatorial ring’, where the largest radius was 0.8 arc-seconds (Bobrowsky 1994; Bobrowsky et al. 1998). The inclination of the ring is 56° . Just inside this ring, a $V=17.0 \pm 0.2$ mag star is a possible wide companion star, making the Stingray a binary with a separation of ~ 2200 AU. The presence of the companion star has been suggested to have some effect on the formation of the bipolar shape, but the very wide separation makes it hard for any such effects to be substantial. Importantly, the visible size of the PN requires an ejection many hundreds or thousands of years ago. Given an angular size of $1.15''$, a distance of 1.6 kpc, and an expansion velocity of 8.4 km s^{-1} from the [OIII] line width, we get a kinematic age of the main PN shell to be 1013_{-793}^{+488} years (Reindl et al. 2014). So we have a clear picture that the PN shell was ejected about a millennium ago, but was only ionized in 1980.

The Stingray has reasonable coverage from around 1920 to the present with ground-based spectroscopic monitoring, from 1988 to 1996 with *IUE* spectra, and from 1992 to 2000 with *HST* ultraviolet spectroscopy and high-resolution imaging. But no one has reported any photometry past a few isolated magnitudes, all with large problems, spread over various magnitude systems. We realized that a full light curve was needed, and we had means for measuring full light curves all the way back to 1889, so as to cover over eight decades of time before the 1980’s ionization event, the transition time of the PN turn-on, and three decades of the coasting phase after the turn-on. Nor has anyone looked for an outer shell far away from the central star (such as are seen around many ordinary PNe), so we wondered whether the Stingray has any far outer shells. This paper reports on our results of the light curve of the Stingray from 1889 to 2015, plus our searches for any outer halo.

2. Photometry

To get broad-band magnitudes for the Stingray, we have pulled from a wide variety of sources; the Harvard photographic plate collection from 1889-1989, the visual magnitude estimates of Albert Jones as archived by the *American Association of Variable Star Observers*

(*AAVSO*) from 1994 to 2007, the *All Sky Automated Survey (ASAS)* from 2001 to 2009, the *AAVSO* telescopes going into the *AAVSO Photometric All-Sky Survey (APASS)* from 2011 to 2015, plus our own photometry from CCD images with DECam on the Cerro Tololo 4-m Blanco telescope from 2014. In all, we have 1026 magnitudes, mainly in B and V, with good coverage from 1889 to 2015. We have added 15 magnitudes from the literature or derived by us from the literature, all on 6 nights from 1969 to 1996. All 1041 magnitudes are presented in Table 2.

A critical realization is that the magnitudes *before* 1980 are all measures of the continuum of the star, while all magnitudes *after* roughly 1989 are essentially measures of the [OIII] emission line strengths. The reason is that before this cutoff date there were no significant emission lines seen in the spectrum so the brightness is of the observed stellar continuum, whereas after that date we see the optical fluxes dominated by emission lines. So before 1980, we are measuring the brightness of the star alone, and this depends only on the effective size and temperature of the photosphere minus any extinction by dust. After 1989, the emission lines dominate, with the brightness depending on both emission line fluxes and the exact spectral sensitivity of the detector. The nebular light in the V-band is entirely dominated by just three emission lines; [OIII] at 5007Å as the brightest with 77% of the V-band detected flux, [OIII] 4959Å with 21% of the flux, and H β at 4861Å as the faintest with only 2% of the flux. So Jones, *ASAS*, and *APASS* are essentially reporting the brightness of the [OIII] emission lines.

A further realization from this is that there will likely be systematic differences in the post-1980’s magnitudes from observer to observer. For example, the exact width of the spectral sensitivity curve for Albert Jones’ eyes is somewhat different from the *ASAS* CCD/telescope/atmosphere combination, so Jones will detect somewhat more [OIII] light relative to what he detects for the nearby comparison stars as compared to the *ASAS* measures. These systematic observer-to-observer offset are real, and apparently at the quarter-of-a-magnitude level.

Another critical realization is that the emission line spectrum for V839 Ara makes its measured brightness respond slightly differently to atmospheric extinction than do the brightnesses of the nearby comparison stars. The reason is that V839 Ara has all of its light on the blue-side of the V-band, while the ordinary comparison stars have a continuum that fairly evenly covers the entire V bandpass. Ordinary atmospheric extinction dims the blue side of the V bandpass more than the red side. Extinction from the ground changes on many timescales due to differing airmass (as the Stingray is looked at with varying zenith distances) and with ordinary changes in the atmosphere aerosol content. Thus, if atmospheric extinction increases for any reason, then the blueish emission light of V839 Ara will be

dimmed somewhat more than the light from the normal comparison stars will be dimmed. All of the ground-based photometry reported here is straight differential photometry with respect to an ensemble of nearby comparison stars, so V839 Ara will appear to slightly dim in our derived V magnitude as the atmospheric extinction increases. This effect cannot be taken out with the usual color terms derived from the comparison stars for the CCD/filter/telescope combination, and indeed, an exact correction is not possible without more information on the atmosphere and spectral sensitivities than is available. So we are left with a relatively small atmospheric source of variability superposed on the real underlying light curve. From the *APASS* time series, we see that the effect can get up to around 0.05 mag in amplitude. For all other ground-based telescopes, we cannot recover from this atmospheric variation, so we just have to acknowledge that the measured magnitudes have a non-astrophysical variability of roughly 0.05 mag superposed. This problem arises from the nearly-unique nature of the Stingray’s emission line spectrum. Importantly, this mechanism does *not* apply to the pre-1980s Harvard magnitudes, because the star dominated with no significant emission lines. Fortunately, for the post-1980s light curve, fast variations are impossible (because the visible light is coming from emission lines spread out over a region one light-month in size), so we can use our many magnitudes to get time-averaged variations with atmospheric effects well-averaged out.

2.1. Harvard Plates

The Harvard College Observatory has a collection of over 500,000 archival photographic plates that cover the entire sky from 1889 to 1953, plus a smaller collection from around 1969 to 1989. (The years 1953-1969 are the notorious Menzel Gap.) These plates are mostly in the B band, with limiting magnitudes typically ranging from 14 to 18 mag. Any one position will have typically from 1000 to 4000 plates for coverage. The *Digital Access to a Sky Century @ Harvard* program (*DASCH*) is currently $\sim 10\%$ through digitizing all the Harvard plates, but it will reach the Stingray (in the constellation Ara at low galactic latitude) only some years from now.

We have constructed a light curve from 108 Harvard patrol plates, all in the B band. The plates were all from the B series as well as on patrol plates of the RB, AM, AX, and DSB series. (We could have measured many more magnitudes for such a bright star as the Stingray, but the patrol plates taken have the complete coverage in time and already well-define the star’s variability, so adding more plates would provide little new information.) The comparison stars were chosen from nearby stars of similar magnitude, with their B magnitudes taken from the *APASS* survey of the *AAVSO*. The Harvard plates formed part of

the original definition of the B magnitude system, and they have been measured many times to have a near-zero color term for transformations from their native system to the Johnson B magnitude system. With this, we can be very confident that our resultant magnitudes are in the Johnson B magnitude system.

The visual comparison of targets to the comparison stars is a long well-developed practice, now largely lost amongst living astronomers. Nevertheless, extensive experimentation over the last thirty years has proven that the visual estimation of magnitudes has an accuracy essentially equal to that obtained from digital scans and from iris diaphragm photometers. Importantly, an experienced eye will produce a real uncertainty that is more than a factor from 1-times to 3-times better than that produced by the *DASCH* photometric pipeline (e.g., Schaefer 2014a, 2014b). Given our very long and deep experience at visual estimation, plus its great speed, simplicity, and low-cost, the visual estimation method is to be preferred. For an average case with a good sequence and a target well above the plate limit (as for the case of the Stingray), the real one-sigma error bar is close to ± 0.10 mag.

The Harvard plates light curve from 1889 to 1989 is presented in Table 2 and Figure 1. The behavior of the Stingray was startlingly unexpected. From 1889 to 1980, the star slowly faded, with significant modulation. The fading is consistent with a linear decline in magnitude, going from $B=10.30$ in 1889 to $B=10.76$ in 1980, for a decline at a rate of 0.0051 mag/year. Superposed on this linear decline are apparent fluctuations on the decadal timescale with a total amplitude of near half a magnitude. Then, starting suddenly around 1980, the Stingray central star faded fast at least until 1989. The rate of decline was approximately 0.20 mag/year.

2.2. Albert Jones

From early 1994 until the middle of 2007, Albert Jones has reported 128 visual measures of the Stingray. These are all visual measures, through his 12.5-inch reflector telescope in Nelson New Zealand, made using a sequence of comparison stars that is accurate on the modern magnitude scale. Thus, his measures are closely on the Johnson V-magnitude system. Jones' magnitudes were reported through the Variable Stars Section of the *Royal Astronomical Society of New Zealand*, and are now available in the *AAVSO* database.

Albert Jones has been the world's best observer of variable stars for much of the last sixty years. (He died in 2013.) Some of his exploits include the discovery of the highly-important SN 1987A, the discovery of two recurrent novae eruptions (T Pyx in 1966 and V3890 Sgr in 1990), and the discovery of two comets. In the early 1990's, Janet Mattei

(then *AAVSO* Director) pointed him out as being the all-time best variable star observer with incredibly accurate eyes, while Daniel W. E. Green (now the Director of the *Central Bureau for Astronomical Telegrams*) pointed him out as being the world’s best observer of comet magnitudes. And he not only has an incredible accuracy, but he also has made over 500,000 variable star magnitude measures, nearly a factor of two times more observations than any other visual observer. The authors of this paper have used Jones’ observations in many prior studies for a wide range of stars, and we have always been deeply impressed by both his quality and quantity of observations, as well as by his characteristic of always looking at the fun, exciting, and useful variables. Results from our prior work, and from others, give Jones as having a one-sigma photometric accuracy of 0.05 to 0.10 mag. The reason for this recital is to point to Jones’ reliability and accuracy.

The RMS scatter of the differences between successive magnitudes in the light curve is 0.21 mag for pairs within 10 days. Jones is only measuring the [OIII] emission lines, and these cannot vary substantially on such fast time scales. (This is because the [OIII] light comes from all around the planetary nebula, with near-zero from the central star, and the nebula is about a light-month in radius.) As 0.21 mag is the difference between two magnitudes, the one-sigma uncertainty for measuring one magnitude will be 0.15 mag. This variation is significantly larger than Jones’ photometric accuracy. So we take the excess variance to be due to the effects of variations in the atmospheric extinction, where the emission lines from V839 Ara are dimmed more than the continuum light from the comparison stars. Thus, the extinction effect is somewhat smaller than 0.15 mag in size.

Jones’ visual light curve is plotted in Figure 2, with circles representing his measures. His light curves shows a steady decline with superposed apparently-random fluctuations. His observations are reasonably fit with a linear decline, from $V=10.71$ in 1994 to $V=11.77$ in 2007, for a decline rate of 0.081 mag/year. The RMS scatter around this linear decline is 0.22 mag.

2.3. ASAS

ASAS has been running an all-sky survey, measuring V magnitudes for approximately 10 million stars on a nightly basis (Pojmanski 2002). The telescopes all have lenses of aperture 200 millimeters and f-ratio of 2.8, forming an $8.5^\circ \times 8.5^\circ$ field of view, while the CCD has a pixel size of $15''$. With 180 second integrations, the limiting magnitude is roughly $V=14$. For observations in V of the Stingray, the telescope is at Las Campanas Observatory in Chile. The publicly available light curve is from early 2001 to late 2009, and we will have 425 V magnitudes.

For the reported *ASAS* V magnitudes, we selected out only the grade A and B values. These magnitudes show a slow secular decline from 2001 to 2009, plus a large scatter superposed on top. Uncrowded neighboring stars of similar brightness show a good flat light curve with an RMS scatter of 0.06 mag. The publicly reported magnitudes are divided into ten blocks, where each block was made with a different field center and slightly different positions for the centers of the photometry apertures. Each field center produces a scattered light curve that parallels the light curves from the other centers, yet the field centers have offsets that vary by 1.6 mag (with an RMS scatter in the intercepts of 0.57 mag). The cause for this variations is that a $V=10.73$ star is $35''$ from the Stingray, so small changes in the center of the photometry aperture will make for a varying contribution from the nearby star. To pull out this effect, we have constructed a model with a presumed Gaussian point spread function (PSF) for the *ASAS* star profiles. For the known aperture radii, the known star positions, and the known centers for the photometry aperture, this model has only one fit parameter, the Gaussian width of the PSF. The *ASAS* literature gives typical values from $10''$ to $15''$ (e.g., Pojmanski 2002). We have made a chi-square fit for the reported brightness for each of the ten field centers and the five aperture diameters ($30''$, $45''$, $60''$, $75''$, and $90''$). Our best fit is with a Gaussian sigma value of $14''$. With this value plus our model, we have derived the V magnitude for the Stingray.

The resultant light curve still shows substantial scatter. For pairs of magnitudes taken within 10 days of each other (so that the nebular [OIII] light cannot vary significantly), the RMS scatter of the magnitude differences is 0.31 mag. The one-sigma measurement uncertainty for one magnitude is 0.22 mag. This large scatter is much larger than dictated by photon statistics. The cause for this scatter can be due to the atmospheric extinction variations (as discussed previously) as well as the circumstance of having imperfect correction for a relatively bright star just near the edge of the photometry aperture. Small variations in the PSF width and the center of the photometry aperture can make for substantial changes in the derived brightness for the Stingray, and we have no way to recover this from the publicly available data.

The *ASAS* light curve from 2001 to 2009 (see Figure 2) shows a steady decline, with this being highly significant despite the substantial measurement errors. This decline is consistent with a linear change in the magnitude, going from 11.41 in 2001.0 to 12.53 in 2010.0, at a rate of 0.124 mag/year. The RMS scatter around this trend line is 0.23 mag.

Figure 2 shows us that the *ASAS* light curve has a similar slope from 2001-2009 as does Jones from 1994-2007, but that there is an offset by 0.2 to 0.4 mag in the overlap time interval. It is possible that our model of the Stingray produced a systematic underestimate of its contribution to the smallest photometry aperture. However, we think that it is more likely

due to Jones and ASAS having different spectral sensitivities. That is, the photochemicals in Jones' eye will produce a distinctly different relative sensitivity for the [OIII] lines (when compared to the mean sensitivity for the continuum from the comparison stars) than will the ASAS CCD-plus-filter. In this case, the observed offset is just the result of normal color terms between two different detectors, with this being exaggerated for an emission line source. In all cases, the photometric uncertainties are below the quarter-magnitude level, and we can easily see the overall behavior of the Stingray.

2.4. APASS

APASS is measuring B, V, g', r', and i' magnitudes of all stars in the sky with approximately $10 < V < 16$, with several telescopes in both the northern and southern hemisphere. This has provided us with a reliable source of comparison stars for our differential photometry. This has also provided us with magnitudes in the five filters on two nights in 2011 (see Table 2).

At our request, A. Henden has put the Stingray in the queue for time series photometry on the 0.61-meter Optical Craftsmen Telescope at the Mount John Observatory in New Zealand. The 1-minute CCD integrations were through a Johnson V filter on the nights of 23, 26, and 27 March 2015. The quoted magnitudes were based on differential aperture photometry with respect to 5-8 nearby comparison stars previously calibrated with *APASS*. On the first night, as the Stingray rose from an altitude of 31° to 54° , the apparent brightness of the Stingray suffered a dip in brightness by about 0.05 mag for one hour. The Stingray was constant, with an RMS scatter of 0.008 mag, on the other two nights. During the time of the dip, the statistical error for the star increased from 0.012 mag up to 0.06 mag, indicating that some large atmospheric extinction had dimmed the target by much more than 0.05 mag. For the time through the dip and for all the nights, we found a tight correlation between the calculated statistical error and the differential magnitude of the target. This has the easy interpretation that ordinary changes in the atmospheric aerosols substantially dimmed both the Stingray and its comparison stars (making for large statistical errors), while the Stingray's [OIII] emission lines (all on the blue side of the V bandpass) were dimmed more than the continuum light from the comparison stars (making for the small dip in the differential magnitude). This effect is undoubtedly happening on all time scales to all ground-based observers, but we can see this effect only in a time series from one telescope. With this correlation, we can reduce all the *APASS* magnitudes to those of some constant condition with minimal aerosols. For the measures with statistical error greater than 0.020 mag, this correction could not be done with high accuracy, so we have chosen to delete these

data. The result is a time series on three nights with 352 V-band magnitudes (see Table 2), with nightly averages of 12.62, 12.57, and 12.61.

The *APASS* magnitudes extends the V-band light curve past 2009 up until March 2015 (see Figure 2). From the *APASS* magnitudes alone, we see a significant decline from 2011 to 2015. This is just a smooth extension of the earlier decline. The various observers are not expected to report the same V magnitudes to within a quarter of a magnitude or so, due to the emission line nature of the Stingray. Nevertheless, all observers show a consistent and highly significant steady fading from 1994-2015. This fading goes from $V=10.71$ in 1994.1 to $V=12.61$ in 2015.3, for an average decline rate of 0.090 mag/year.

2.5. DECam on Cerro Tololo 4-m

With the Cerro Tololo 4-meter Blanco Telescope, DECam CCD images were taking on 30 June 2014, the main goal being to search for any outlying faint optical shell. The large size ($9' \times 17'$) of one individual chip allows for V839 Ara, comparison stars, and for any far out shell to be contained on a single CCD (out of the 64 CCD array). Observations were made using the the u' , g' , r' , i' (which are the Sloan Digital Sky Survey, SDSS, filters) with pairs of exposure time of 20 and 90 seconds in each band.

Standard procedures were used in the IRAF data reduction package to extract magnitudes for V839 Ara utilizing the PHOT package. Differential photometry was performed on V839 Ara using multiple *APASS* comparison stars, carefully avoiding saturated stars, and only with the short exposures. These comparison stars were chosen such that they fell on the same chip as V839 Ara, have similar brightness, and not crowded by surrounding stars. Since *APASS* only provides information for g' , r' , & i' filters, a magnitude for the u' observations could not be derived. We measured the magnitudes of V839 Ara to be 12.52 ± 0.01 , 12.18 ± 0.01 , & 13.35 ± 0.01 for g' , r' , & i' respectively. The formal statistical error bars are smaller than 0.01 mag, while various systematic sources of error are likely around the 0.05 mag level.

2.6. Additional Optical Magnitudes

Hill et al. (1974) and Kozok (1985a) report on UBV photometry on four separate nights. These magnitudes are of the central star, with any contributions from emission lines and the PN being negligibly small. These four B magnitudes closely fit with the light curve from the Harvard plates.

Bobrowsky et al. (1998) used *HST* to resolve the central star and report $V=15.4$ as deduced from the flux measured in a continuum filter centered at 6193\AA . This magnitude is of the central star alone (with no emission lines and no PN shell) was made in March 1996. Around this time, Albert Jones was reporting the Stingray to be $V=10.8$ mag. The difference of 4.6 mag is because Jones is including the shell light, almost entirely [OIII] emission lines. This shows that the two [OIII] lines are contributing $\sim 70\times$ as much flux as the star over the entire broad V-band.

Reindl et al. (2014) report on an *HST* spectrum from March 1996 with the *FOS*. We have taken the continuum flux for the center of the B- and V-bands, and converted these into magnitudes. We get $B=14.64$ and $V=14.96$, with this applying to the star alone. The V magnitude is 0.44 brighter with the *FOS* spectrum than with Bobrowsky’s continuum flux, despite there being only two days of separation in time. It is unclear if the difference arises from variability or from the ordinary uncertainties in extracting magnitudes with two different non-standard methods.

Other published magnitudes (like the estimates from the *Cape Durchmusterungen* and *HD* catalogs) have problems with their comparison stars that can be as large as one magnitude, and hence cannot be used with any useful accuracy or confidence. The presentation of the *ASAS* magnitudes by Arkhipova et al. (2013) has not realized any of the problems or solutions caused by the varying centers and the nearby star, so their light curve is now to be replaced by our light curve described in Section 2.3.

2.7. Infrared and Radio Brightnesses

From the 1992 Ph.D. thesis of P. Garcia-Lario (as quoted in Parthasarathy et al. 1993) the J, H, and K magnitudes were 11.37, 11.97, and 11.38. These magnitudes presumably date from around 1991. Like all the brightnesses in this subsection, these refer to the entire nebula, with near-zero contribution from the central star.

The *2MASS* magnitudes were $J=12.098\pm 0.034$, $H=12.248\pm 0.048$, $K=11.506\pm 0.029$ (Cutri et al. 2003). The magnitudes are from May 2000.

The *IRAS* fluxes were 0.65 Jy at 12μ , 15.59 Jy at 25μ , 8.05 Jy at 60μ and 3.39 Jy at 100μ (Parthasarathy & Pottasch 1989). These observations were made from January 1983 to November 1983. This spectral energy distribution has the obvious interpretation as thermal emission from dust in the shell, with an average temperature of 125 K (Parthasarathy & Pottasch 1989).

The *Akari* satellite all-sky survey gives the 9μ flux to be 0.089 ± 0.009 Jy and the 18μ flux to be 2.57 ± 0.05 Jy (Ishihara et al. 2010). These brightnesses come from a survey running from May 2006 until August 2007.

The *WISE* all-sky survey provides magnitudes (on the Vega magnitude system) for the various WISE bands to be 11.144 ± 0.0022 , 10.373 ± 0.019 , 5.161 ± 0.014 , 0.902 ± 0.01 for the W1 (3.4μ), W2 (4.6μ), W3 (12μ), and W4 (22μ) bands respectively. The *WISE* survey ran from January 2010 to January 2011.

The *ATCA* radio light curve, from 1991 to 2002, has the Stingray declining steadily in flux density from 63.6 ± 1.8 mJy (Parthasarathy et al. 1993) to 48.8 ± 1.5 mJy at 4800 MHz (Umana et al. 2008).

3. Images

Roughly 50% of classical PN have halos, faint roughly-circular shells far outside the the bright well-known nebulosity (Chu et al. 1987). For example, NGC 6720 (the famous Ring Nebula) has the obvious shell (with outer dimensions $90''\times 65''$) surrounded by a faint shell extending $162''\times 147''$ filled with fairly uniform mottling and arcs, with this outer halo being bright in *WISE* images. Corradi et al. (2003) and Chu et al. (1987) have catalogs with pictures and intensity profiles. The typical surface brightness is a thousandth of that of the inner classical PN. The estimated ages for these outer shells are many tens of thousands of years as based on expansion velocities that default to 20 km s^{-1} when not otherwise known. Corradi et al. (2003) call these faint shells structures outside the classic PN as ‘AGB halos’, where the ordinary stellar wind of the star during its AGB phase has become ionized. They claim that the outer edge of the AGB halo results from the last thermal pulse in the AGB star.

It is possible that the Stingray might have an AGB halo outside its small classical PN shell. Such a shell might be too large to be visible in the *HST* images. So we thought it worthwhile to search for any AGB halo around the Stingray. We examined deep images from DECam, SHASSA, 2MASS, and *WISE*, as reported below. We have also examined the various available images from the Digital Sky Survey and from *HST*, but our negative results for any shell structure or circular arcs centered on the Stingray do not provide useful constraints. No images were taken with *GALEX* or *Swift*.

3.1. DECam Images

Our DECam images in u' , g' , r' , and i' were examined for any nebulosity surrounding the Stingray. In our images, the classical planetary nebula is entirely in the near-saturated inner core of the normal stellar image. So we are only sensitive to any outlying outer shell. Our examination was visual, mainly because there is no way to automate or quantify a shell search when we have no idea of the size or shape. We have very long experience at searching for shells or light echoes around stars, and we know that the human eye/brain combination is very sensitive to detecting shells. Indeed, for irregular shells, visual examination is greatly better at detecting any nebulosity by pushing down towards the background noise limit. With this, we detect no shell or nebulosity in any of our DECam images. The r' image would record any $H\alpha$ emission, while the g' image would record any [OIII] emission.

3.2. SHASSA Images

The Southern H-alpha Sky Survey Atlas (SHASSA) is a robotic wide-angle CCD survey in the $H\alpha$ line covering declinations south of $+15^\circ$ (Gaustad et al. 2001). Images have pixels that are 47.64 arc-seconds on a side, with a sensitivity down to about 0.5 Rayleigh. The Stingray appears prominently about 4° from the center of their Field 38. The point-spread-function has a FWHM of around 1 arc-minute, so all the known shell appears as a point source, and any detectable shell would have to be larger than several arc-minutes in radius. The continuum-subtracted and smoothed image shows no shells, circular arcs centered near the Stingray, or any structure associated with the Stingray out to a radius of over 1 degree.

3.3. 2MASS Images

There are also 2MASS observations of V839 Ara in J, H, and K bands taken in May of 2000. The radius of emission in each of these three bands are less than $3''$. No outer shell was seen in J, H, or K.

3.4. WISE Images

The archival *WISE* images covers V839 Ara in four different bands centered on $3.3\mu m$ (W1), $4.6\mu m$ (W2), $12.1\mu m$ (W3), and $22.2\mu m$ (W4). V839 Ara is positioned nearby a star (identified as TYC 8739-1088-1 with $V=10.83$) which is bright in both the W1 and

W2 bands, however, it is noted that PNe are expected to show strong emissions in the far infrared. In the W1 band, the emission is centered on the location of V839 Ara with a radius of 11". Going further out into the infrared, the emission centered on V839 Ara extends out to a radius of 14" in W2, 34" in W4, and a finally a very large ‘halo’ with a radius of 81" in W4. It should be noted that this ‘halo’ seen out in $22\mu\text{m}$ is consistent with PSF rings around sources bright in the W4 band, and is not astrophysical. This can be seen in Figure 3.

4. Light Curve Analysis for the Central Star

From 1889 to 1980, the Stingray’s central star exhibits a linear decline in its light curve, with substantial variability superposed. The best fit line goes from 10.30 mag in 1889 to 10.76 mag in 1980, for a total drop of 0.46 mag. This is the same as the apparent amplitude for the decade-long variations. Over this time, with no substantial emission lines providing any significant fraction of the flux, the variability can only be caused by changes in the photosphere, either by variations in the effective temperature or radius. (Changes in the dust column seem unlikely given that the stellar wind must be weak, while even large winds in the 1980’s led to no change in the extinction.) From *c.*1920 to 1980, the spectral type remained largely unchanged, with everyone reporting spectral types from B0 to B3, so the star’s surface temperature was not changing by any large factor. For the B-band flux to change by 0.46 mag, the radius would have to change by 20%. This is a large change.

How can the Stingray star have ‘anticipated’ the 1980s ionization event? Apparently, some prelude to the sudden event had a surface manifestation for at least a century in advance. The anticipation cooling and/or shrinking of the central star could not have been going on for many centuries. At its rate of fading by near half-a-magnitude per century, a millennium duration would imply that the central star was five magnitudes more luminous at the start of the anticipation. Such would imply a luminosity higher than supergiants. So this anticipation fading can only have been going on from one century to a few centuries. Detailed calculations of the variations of the central star luminosity can have substantial changes in the century preceding thermal pulses (Blocker 1995; Schönberner 1983). For a $0.553 M_{\odot}$ star, before a thermal pulse at 45,000 K, the luminosity will drop by a factor of 2.2 in the preceding century (Schönberner 1983). For a $0.836 M_{\odot}$ star, the luminosity will drop by a factor of 6 in the century preceding a thermal pulse at 200,000 K (Blocker 1995).

Handler (2003) has defined a new class of variable stars, called the ‘ZZ Leporis’ stars, which consist of the central stars of young PN with temperatures $<50,000$ K. The physical mechanism for these brightness changes is not known, but it is likely some combination of

stellar pulsations and fluctuations in a stellar wind. Arkhipova et al. (2013) have already identified the central star of the Stingray as being in this ZZ Lep class. However, although the variations are fast and aperiodic in both cases, the ZZ Lep stars have greatly different light curve properties than what we see for the Stingray. In particular, ZZ Lep stars have time scales of 4-10 hours and amplitudes <0.03 mag (Handler 2003; Handler et al. 2013). This is greatly different from the Stingray’s behavior in 1889-1980, which has a time scale of around one decade and amplitude 0.5 mag. From 1994-2009, our V-band light curve is not coming from the central star, while the central star may or may not have ZZ Lep behavior.

The fast decline for the light from the central star alone from 1980 (B=10.8) to 1988.5 (B=12.5) to 1996.3 (B=14.64) is stark and unprecedented. This cannot be due to changing extinction, because the dimming, as measured by many methods, is essentially unchanged from 1980 to 2011 (Reindl et al. 2014). So this fast fading star can only be due to some combination of the decrease of the stellar radius and a decrease in the temperature. For the case of the Stingray, Reindl et al. (2014) show that the stellar temperature increased greatly while the star’s radius decreased greatly from 1988 to 2006. The radius and temperature changes run against each other. So it takes a detailed calculation as to whether these observed changes translate into the observed magnitude changes. If we go by the usual luminosity equation, we have $L \propto R^2 T_{eff}^4$, where L is the luminosity, R is the stellar radius, and T_{eff} is the effective temperature of the photosphere. We do not have direct measures of the radius, but the star’s surface gravity, g , will scale as $g \propto R^{-2}$. And we should not be using the luminosity, but rather the blackbody flux in the B-band, F_{BB} , at $\lambda=4400\text{\AA}$, with this being the usual Planck function of λ and T_{eff} . We can then get a B magnitude as $B = B_0 - 2.5 \log(F_{BB}/g)$, for some zero magnitude B_0 . Reindl et al. (2014) list measured values for $\log(g)$ and T_{eff} for many years from 1988 to 2006. Taking $B_0 = 43.55$ so that B=12.5 in 1988, we get B=13.1 mag in 1996, and B=14.9 in 2006. We see that in this case for a shrinking star that is getting hotter, it is the shrinking that is the dominant effect, making for the star dropping in B-band brightness. However, the effect predicted from the measured $\log(g)$ and T_{eff} is a much slower decline that is actually observed. That is, from 1988 to 1996, the prediction is that the central star will dim by 0.6 mag, while the observed dimming is by 2.14 mag. This is a large difference. This points to the central star having additional light above the photosphere in 1988 that went away by 1996, or to changing systematic errors in measures of the surface gravity (perhaps associated with the changing stellar wind rate). From this analysis, we take the basic cause for the fading of the central star to be due to the shrinking of the stellar radius, although detailed calculations do not predict the central star to be fading as much as is observed.

5. The Fading Nebula

The V-band light curve (essentially the nebula’s brightness) from 1994 to 2015 has been steadily fading at the rate of 0.090 mag/year. This is a highly significant result from three independent sources and has no prospect of being due to any artifact. So we have the [OIII] emission line flux fading with a half-life of around 8 years. From 1994 to 2015, the Stingray emission lines have faded by near 2.0 mag, a factor of near $6\times$. This is the nebula fading, not the central star.

The fading of the nebula is also seen for wavelengths from the near infrared, the middle-infrared, and the radio: (1) From around 1991 to 2000.4, the Stingray faded by 0.73, 0.28, and 0.13 mag for the J, H, and K bands respectively. These correspond to half-lives of 9.3, 24, and 54 years respectively. (2) We can use the *IRAS*, *Akari*, and *WISE* mid-IR fluxes to chart the changes in the 12μ flux. For this, the *WISE* magnitude must be converted to Jansky, and the *Akari* flux must be interpolated to 12μ . With this, we have 12μ fluxes of 0.65 Jy in 1983.5, 0.36 Jy in 2007.0, and 0.226 Jy in 2010.6. This shows a steady decline over 27.1 years with a half-life of 20.4 years. (3) Similarly, for 22μ , we have fluxes of 8.96 Jy in 1983.5 and 3.20 Jy in 2010.6. The extrapolation of the *Akari* 18μ flux to 22μ is just where the spectral energy distribution is turning over, so the uncertainty is too large for this to be useful. This shows a decline in flux with a half-life of 18 years. (4) From 1991.3 to 2002.7, the ATCA radio flux at 4800 MHz (6 cm) declined from 63.6 mJy to 48.8 mJy. This corresponds to a half-life of 30 years.

We see a consistent picture for the light curves from 1994-2015, where the optical, near infrared, middle-infrared, and radio fluxes have all been smoothly fading with a characteristic time scale of a decade or so. The nebula had a sudden turn-on sometime between 1979.49 and 1988, and the brightening of the nebula likely stopped in the early 1990’s with the turn-off of the fast stellar wind associated with the 1980s ionization event. The fading of the nebula started after the end of the ionizing event and its fast stellar wind, in the early 1990s. At this time, the central star underwent fast fading (see Figure 1), so its illumination of the nebula started to decline fast. It is easy to ascribe the fading of the nebular light to the sharp fall off in its illumination by the central star. Even with the rise of surface temperature of the star, the fall in its surface area means that it is giving off much less ionizing radiation. With the turnoff of the illuminating source, the nebula light should start fading at some sort of a re-ionization time scale. There is precedent for this fading and this interpretation for Sakurai’s Object (V4334 Sgr, a very-late-thermal-pulse born-again star). Its emission line fluxes have also been seen to decline fairly rapidly (with a half-life just under two years) from 2001 to 2006, with the fading attributed to cooling and recombination in the shell after the heating and ionization ended (van Hoof et al. 2007).

For the usual nebula conditions, the recombination time scale is around 80,000 years divided by the electron number density (in units of cm^{-3}). (The nebula will have a range of densities, each recombining and fading on their own time scale, with continual-but-fading illumination from the central star, so the connection between the average electron density and the effective recombination times and the fading rate has substantial uncertainty and change over time.) For the Stingray, Parthasarathy (2000) gives an electron density of $10,000 \text{ cm}^{-3}$, so we expect a recombination time scale of around 8 years. The agreement between the half-life for the fading of the optical emission lines and the recombination time scale is an indication that the slow steady fading of the nebular light from 1994-2015 is caused by the ordinary recombination inside a nebula that had some sort of an ionization event between 1980 and 1994.

The middle infrared emission is dominated by thermal light from warm dust in the nebula. The dust grains are not likely to be changing in number or size, so the thermal flux can only be fading due to a cooling of the dust grains. This is all consistent with a scenario where the dust was heated during the 1980s ionization event and has been cooling ever since. The dust reaches thermal equilibrium on a fast time scale, so the fading of the middle infrared emission is a measure of the fading of the heating radiation field. We suggest that the dust heating is dominated by the nebular emission lines, with this being *in situ* and the connection is made because the nebular lines are fading at the same rate that the dust is fading.

The radio emission is free-free light, with model derived electron densities of $1.23\text{-}2.5 \times 10^4 \text{ cm}^{-3}$ (Parthasarathy et al. 1993; Umana et al. 2008). Like for the optical line emission, with a scenario of a short-duration ionization event in the 1980s, the radio flux should fade on some sort of a recombination time scale.

6. Evolution Through the HR Diagram

With the results from this paper, we can construct a detailed evolutionary path of the Stingray through the HR diagram. For seven dates, we have calculated L and T_{eff} for the central star (see Table 3). These can be directly plotted onto the HR diagram and compared to model predictions (see Figure 4). The first point, labeled for the year 1001 AD, is meant to illustrate the approximate position where the star ejected the PN shell, just as it was leaving the AGB phase. This is useful to show that the Stingray took only around one millennium to cross from the AGB to the thermal pulse region. The two points for 1889 and 1980 have a modest uncertainty from the distance, so they can be moved up or down in the diagram, but they must be moved up or down together. Similarly, the last four points can

be moved up and down together by modest amounts as the assumed stellar mass changes from the adopted $0.55 M_{\odot}$. The end result is an observed evolutionary path from when the Stingray leaves the AGB until sometime during a thermal pulse.

The default or common idea is that the Stingray central star has evolved off the AGB with the usual nearly horizontal path across the top of the HR diagram (e.g., Parthasarathy et al. 1993), and is now undergoing a late thermal pulse (e.g., Reindl et al. 2014). (See the next section for possible alternatives.) Late thermal pulses are when a shell of helium, just outside the carbon-oxygen core, is ignited, with the energy from this burning making the star temporarily increase back to giant size, with the result that the star forms a loop in the HR diagram. Detailed evolutionary paths through the HR diagram depend on the stellar mass, while the thermal pulses can occur anywhere along the path (e.g., Schönberner 1983; Blocker 1995; Blocker 2001; Schönberner 2008). For illustrative purposes, one such late thermal pulse evolutionary track (from Schönberner 1983) has been superposed on the Stingray’s observed evolutionary track in Figure 4. This track was chosen because it is for a stellar mass that might be similar to that of the Stingray, because the thermal pulse is at a similar temperature as for the fast evolution of the Stingray, and because the track has conveniently labelled time tick marks to allow direct comparison.

The comparison between the observed and theoretical evolutionary paths in Figure 4 shows fundamental problems: (1) The time scale for the evolution from a temperature of order 5000 K (when the PN shell was ejected) to a temperature of 50,000 K (in 1996) is observed to be around one millennium, while theory dictates a time scale more like 13 millennia to cross from roughly 5000 K to 50,000 K. This discrepancy can be resolved if the star is greatly more massive than $0.55 M_{\odot}$, but this then raises other difficult discrepancies. (2) The Harvard plates show the Stingray was fading from 1889 to 1980, while the spectra from 1920 to 1979.49 show a nearly-unchanging spectral type, so we have a distinct vertical segment on the HR diagram lasting about a century. From the theoretical paths, this could only match the initial turn in to a thermal pulse, like from the tick marks “13” to “13.1” in the theoretical path shown in Figure 4. But if this match be made, then the further observed path to 1988-2006 is mystifying. (3) The Harvard plates show a sharp drop in the central star’s luminosity from 1980 to 1988, all with the temperature not changing greatly, so we must have another connected nearly vertical segment which lasts only 8 years. This segment does not match any theoretical segment, in particular because its 8 year duration (0.008 millennia for comparison with the theoretical tick marks) is many orders-of-magnitude faster than any expected evolution, even for a massive star. (4) The 1988-1996-2002-2006 segment shows significant and complex evolution. In under two decades, the central star has moved in the HR diagram by more than theoretical paths allow for within two centuries at its fastest. And the total change in luminosity from 1889 to 2006 (around 1.65 in log-units)

is greatly larger than allowed in theoretical models.

7. Fundamental Problems

We can point to two major discrepancies between measures of fundamental parameters for the Stingray: First, the mass of the star has contradictory evidence pointing to $0.55 M_{\odot}$ (Parthasarathy et al. 1995), $0.59 M_{\odot}$ (Bobrowsky 1994), $0.354^{+0.14}_{-0.05} M_{\odot}$ (Reindl et al. 2014), or $0.87 M_{\odot}$ with an initial mass up to $6 M_{\odot}$ (Reindl et al. 2014). Second, the variations in the measured temperature and surface gravity for the central star *qualitatively* reproduce the sharp decline in brightness from 1980 to 2006, but *quantitatively*, the predicted decline from 1988 to 1996 is 0.6 mag, in stark contrast to the observed 2.14 mag decline (Section 2.6).

A fundamental problem posed by the Stingray is the nature of the 1980s ionization event. We have seen no paper that addresses the question of what is really going on during this event, likely because answers are not known to the fundamental questions. (1) Why should the ionization event start so suddenly within a time scale of a few years? The evolution time scale for the increase in ionizing flux resulting from a simple transit across the top of the HR diagram is many millennia, while the evolution time scale for a thermal flash is centuries and longer. (2) What is the physical mechanism that makes for the high luminosity of ionizing flux? Presumably the pre-existing shell was ionized by ultraviolet or far-ultraviolet radiation, and such might come from the central star getting hotter. But the surface temperature of the star only changed from around 30,000 K (from 1920-1979.49) to 38,000 K (in 1988), and we need a detailed calculation to see whether such a modest temperature change can make the nebula evolve from only weak Balmer emission lines to domination of the spectrum by very bright high-ionization emission lines. In any case, the simple use of the central star to provide the ionizing flux does not work because it heated to 60,000 K in the year 2002, but the shell was already fading due to recombination. (3) Why is the ionization event concurrent with the fast and heavy stellar wind as seen from 1988 to the early 1990s? The time coincidence between wind and ionization strongly implies a causal connection. But did the wind make the ionizing radiation, or did the ionizing radiation drive the wind? (4) Why did the ionization event not produce any temporary brightening in the B-band light curve? A mechanism that suddenly produces a large luminosity of ultraviolet light will almost-certainly produce blue light, but there is no flare in the Harvard light curve with good resolution throughout the entire time period when the flare should occur. (5) Why should the duration of the ionizing event be less than one decade and why should the turn-off time be only a few years? All the evolution time scales are much longer than a

decade.

A higher fundamental problem of the Stingray is the overall nature of its evolution. The general answer is that the star must be somehow traversing the HR diagram to go from the AGB phase to the upper left where it will soon enough end up moving down the white dwarf cooling track. But the simple right-to-left traverse of the HR diagram (as depicted in textbooks) cannot explain the fast and complex evolution of the Stingray’s central star (see Figure 4 and Table 3). So either some additional mechanism is superposing some complex evolution, or the Stingray is not the post-AGB star that it seems. Here, we will briefly discuss three possibilities:

The first possibility to the nature of the Stingray’s evolution is that it is an ordinary post-AGB star undergoing some sort of a thermal pulse, wherein a layer near the surface of the star suddenly ignites nuclear burning, and this influx of energy will puff up the star’s outer envelope to giant portions. Thermal pulses will make a star appear to go through loops in the HR diagram. Perhaps the Stingray is caught just at the time of a thermal pulse, already having completed part of the loop? Thermal pulses come in two types, called ‘late thermal pulses’ (LTP) and ‘very late thermal pulses’ (VLTP). The later starts only after hydrogen burning has become extinct, and a critical feature of distinction is that the stellar surface is virtually free of hydrogen (Schönberner 2008). The known VLTP examples are V605 Aql, Sakurai’s object (V4334 Sgr), and perhaps FG Sge (Lawlor & MacDonald 2003; Schönberner 2008). But the Stingray certainly cannot be a VLTP star because it has only evolved off the AGB by roughly a millennium (when it ejected the PN shell), and because the central star has high abundance of hydrogen (as shown by the prominent Balmer absorption lines visible before 1980). So for this solution, the Stingray would have to be an LTP star. The LTP can make the star trace out a wide variety of loops through the HR diagram (Schönberner 1983; Blocker 1995; Blocker & Schönberner 1997; Van Winckel 2003). In an extreme case (see Figure 2 of Blocker & Schönberner 1997), the star’s track has nine reversals of direction in the HR diagram. For all these published loops, none match the observed track of the Stingray, as detailed in the previous section. None of the published LTP tracks can account for the Stingray, and this is the fundamental problem. Part of this fundamental mismatch between observation and model is that the Stingray is moving in the HR diagram at much faster rates than is allowed by theory. Gesicki et al. (2014) has found similar problems in accounting for the white dwarf mass distribution, and they have had to postulate an acceleration by a factor of 3 in the evolutionary time scales of Blocker (1995). In his major review on post-AGB stars, Van Winckel (2003) says ”the detailed description of the badly known external post-AGB mass loss on top of the mass loss from the nucleosynthetic consumption is crucial for the transition time estimates” for the star crossing the HR diagram in various phases. It might yet be possible for some new model calculation to match the

Stingray’s evolution, but until then, the LTP idea has a fundamental problem.

The second possibility is that the Stingray is a product of a common envelope ejection of the outer envelope of a giant star. That is, in ordinary binary evolution involving a red giant star, a binary can get entangled inside a common envelope, the stars will spiral close together, and the main sequence star can eject the outer envelope of the red giant, leaving a bare stellar core. The ejected envelope will expand, and the hot red giant core will ionize the shell. Reindl et al. (2014) suggested this post-common-envelope (post-CE) state for the Stingray, with the evidence being that the apparent luminosity was consistent with the models of Hall et al. (2013). Hall et al. make a variety of predictions that can be used to distinguish the post-CE systems. (1) The luminosity of the post-CE stars will always be less than about $3.16 \times 10^3 L_{\odot}$ while traversing across the HR diagram from right to left. In sharp contrast, the Stingray had a luminosity of $5.4 \times 10^3 L_{\odot}$ in 1889. It is only after the central star has faded by an order-of-magnitude does the observed luminosity come into agreement with the post-CE tracks. It is possible to overcome this argument by merely having the Stingray at a closer distance, with <1.2 kpc being adequate and within the uncertainty for the distance. (2) The post-CE central star would be a close binary with an orbital period from a fraction of a day up to weeks. We know of no observational tests for this prediction. (3) The evolution through the post-CE phase is greatly slower than for an LTP. Hall et al. calculate that the time scale from the ejection of the shell until the central star is 30,000 K is around 10,000 years, while the time scale for the small turn in the motion along the HR diagram (with the central star hotter than 30,000 K) is 0.1 to 10 million years. This model prediction is greatly against the observed time scales of one millennium from ejection to 30,000 K and decades for the Stingray to turn around in the HR diagram. The stark failure of this post-CE model prediction makes for a strong argument against the second possibility.

The third possibility is that the Stingray is not a PN at all, but is rather a ‘PN mimic’ (see Frew & Parker 2010 for a review). This has been casually suggested by Zijlstra (2015) in just one short sentence. A PN mimic is a star with a surrounding ionized shell that does not come from the ejection of the outer envelope of an AGB star. PN mimics include Wolf-Rayet stars, ‘young stellar objects’, symbiotic stars, B[e] stars, Herbig-Haro objects, reflection nebulae, diffuse HII regions, old novae, and supernova remnants. With such a wide diversity of mimics, it is difficult to absolutely reject all mimic classes for the Stingray. Nevertheless, the observed properties of the Stingray have little in common with any of the classes of mimics. In detail, Frew & Parker point out how optical emission line ratios can discriminate between a typical PN and the various types of mimics. For this, taking the line fluxes from Parthasarathy et al. (1993), for the particular lines as defined by Frew & Parker, we have $\log(F_{H\alpha}/F_{[SII]})=1.83$, $\log(F_{H\alpha}/F_{[NII]})=0.48$, $\log(F_{[NII]6584\text{\AA}}/F_{H\alpha})=-0.59$, and $\log(F_{[OIII]}/F_{H\beta})=0.97$. With these, we can look in their Figures 4 and 5, seeing that

the Stingray is right in the middle of the PN region, and is far away from the various mimic class regions. That is, the Stingray’s emission line spectrum is a classical PN spectrum, and greatly different from the mimics. Further, many properties of the Stingray are characteristic for PNe and are not found in many classes of mimics; including the position of the central star on the HR diagram near B1 II, a classic bipolar point-symmetric shaped shell, the ~ 10 km s^{-1} expansion velocity of the shell, dust with a temperature of 125 K, thermal free-free radio emission, a distance of around 340 pc from the galactic plane, and the lack of any nearby ISM clouds or young stars. With all this, we have strong confidence that the Stingray is not a PN mimic.

After considering all proposals for the nature of the Stingray’s evolution, we have eliminated all but one, with the remaining idea being the common idea that the Stingray is a post-AGB star traversing the upper HR diagram while undergoing some sort of a thermal pulse. The fundamental problem is that there is no published model for a thermal pulse that come anywhere near the fast time scale for evolution or the large vertical motion in the HR diagram.

8. Critical Observations

We can propose four sets of observations that are currently ongoing or feasible in the near future. First, it would be good to get optical and ultraviolet spectra of the shell and the central star, so as to measure the temperature while keeping up with the fast evolution of the system. For this, a program with the *HST* in Cycle 22, with N. Reindl as the principal investigator, will get near- and far-ultraviolet spectroscopy with the *COS* instrument. Second, further *HST* images in 2016 would provide a long enough time baseline so as to measure an accurate expansion age for the ordinary PN shell. These same *HST* images might show the fast wind from the 1980s event. This short duration wind has a velocity and total mass like that of the shell ejected by the recurrent nova T Pyx, for which we see the impact of the wind onto a prior more-massive shell (Schaefer, Pagnotta, & Shara 2010). So we might expect to see this impact lighting up the inside of the old PN shell with bright emission lines. New *HST* images will also allow for resolving the central star and placing it onto the HR diagram, so we can see the evolution from 2006-2016. For this second set of observations, we have just been awarded time during Cycle 23 of *HST*, with Z. Edwards as principal investigator, to use the *WFC3* to take all these needed images. Third, the outer halo of the Stingray can be sought in the radio regime (c.f. Oetli et al. 2015). Fourth, time series spectra exposed to show photospheric absorption features of the central star might show a sinusoidal radial velocity curve that will discover a close-in companion

star (as needed to shape the bipolar nebula) as well as define the separation and mass of the close-in companion. This observing task could also discover a close binary remnant of a post-CE system.

This research has made use of the *APASS* database, located at the *AAVSO* web site. Funding for *APASS* has been provided by the Robert Martin Ayers Sciences Fund. We thank A. Henden for help in getting the *APASS* time series. We thank H. Bond and M. Parthasarathy for comments on our manuscript.

REFERENCES

- Arhipova, V. P., Ikonnikova, N. P., Kniazev, A. Yu., & Rajoelimanana, A. 2013, *Astronomy Letters*, 39, 201
- Blocker, T. 1995, *Ap&SS*, 275, 1
- Blocker, T. 2001, *A&A*, 299, 755
- Blocker, T. & Schönberner, D. 1997, *A&A*, 324, 991
- Bobrowsky, M. 1994, *ApJLett*, 426, L47
- Bobrowsky, M., Sahu, K. C., Parthasarathy, M., & Garcia-Lario, P. 1998, *Nature*, 392, 469
- Chu, Y.-H., Jacoby, G. H., & Arendt, R. 1987, *ApJSupp*, 64, 529
- Corradi, R. L. M., Schönberner, D., Steffen, M., & Perinotto, M. 2003, *A&A*, 340, 417
- Cutri, R. M., Skrutskie, M. F., van Dyk, S., et al. 2003, *VizieR Online Data Catalog*, 2246, 0
- Drilling, J. S. & Bergeron, L. E. 1995, *PASP*, 107, 846
- Feibelman, W. A. 1995, *ApJ*, 443, 245
- Fresneau, A., Vaughan, A. E., & Argyle, R. W. 2007, *A&A*, 469, 1221
- Frew, D. J. & Parker, Q. A. 2010, *PASA*, 27, 129
- Gaustad, J. E., McCullough, P. R., Rosing, W., & Van Buren, D. 2001, *PASP*, 113, 1326

- Gesicki, K., Zijlstra, A. A., Hajduk, M., & Szyszka, C. 2014, *A&A*, 566, A48
- Hall, P. D., Tout, C. A., Izzard, R. G., & Keller, D. 2013, *MNRAS*, 435, 2048
- Handler, G. 2003, in *Interplay of Periodic, Cyclic, and Stochastic Variability in Selected Areas of the H-R Diagram*, ed. C. Sterken (ASP Conference Series, vol. 292), pp. 183-190
- Handler, G., Prinja, R. K., Urbaneja, M. A., Antoci, V., Twicken, J. D., & Barclay, T. 2013, *MNRAS*, 430, 2923
- Henize, K. 1976, *ApJSuppl*, 30, 491
- Hill, P. W., Kilkenny, D., & van Breda, I. G. 1974, *MNRAS*, 168, 451
- Ishihara, D., Onaka, T., Kataza, H. et al. 2010, *A&A*, 514, A1
- Kozok, J. R. 1985a, *A&AS*, 61, 387
- Kozok, J. R. 1985b, *A&AS*, 62, 7
- Oetl, S., Kimeswenger, S., & Zijlstra, A. A. 2015, *A&A*, in press, see arXiv:1403.6715
- Parthasarathy, M. 2000, *Bull. Astron. Soc. India*, 28, 217
- Parthasarathy, M. & Pottasch, S. R. 1989, *A&A*, 225, 521
- Parthasarathy, M., Garcia-Lario, P., Pottasch, S. R. et al. 1993, *A&A*, 267, L19
- Parthasarathy, M., Garcia-Lario, P., de Martino, D. et al. 1995, *A&A*, 300, L25
- Pojmanski, G. 2002, *Acta Astronomica*, 52, 397
- Reindl, N., Rauch, T., Parthasarathy, M. et al. 2014, *A&A*, 565, 40
- Schaefer, B. E. *BAAS*, 223, 209.01
- Schaefer, B. E. *BAAS*, 224, 110.01
- Schaefer, B. E., Pagnotta, A., & Shara, M. M. 2010, *ApJ*, 708, 381
- Schönberner, D. 1983, *ApJ*, 272, 708
- Schönberner, D. 2008, in *Hydrogen-Deficient Stars*, K. Werner and T. Rauch eds (ASP Conference Series, vol. 391), pp. 139-149

Umana, G., Triglio, C., Cerrigone, L., Buemi, C. S., & Lato, P. 2008, MNRAS, 386, 1404

Van Hoof, P. A. M., Hajduk, M., Zijlstra, A. A. et al. 2007, A&A, 471, L9

Van Winckel, H. 2003, ARA&A, 41, 391

Volk, K. M. & Kwok, S. 1989, ApJ, 342, 345

Zijlstra, A. 2015, Rev. Mexicana A. & A., in press, see arXiv:1506.05508

Table 1. Stingray timeline

Year	Reference	Event
c. 1001	Reindl et al. (2014)	Ejection of visible PN shell (assuming 8.4 km/s velocity)
1889	Section 2.1	B=10.1, fading by 0.0051 mag/year for 1889-1981
c. 1920	HD catalog	B0 spectrum, no emission lines
c. 1950	Henize (1976)	H α emission line only, no O[III]
1971	Parthasarathy et al. (1995)	B1 or B2, class I or II, only emission is very weak H β
1979.49	Drilling & Bergeron (1995)	O or B spectrum, no emission line
1980	Section 2.1	B=10.8, starts fast fade at 0.20 mag/year
1988.5	Section 2.1	B=12.5, central star is fading fast
1988	Feibelman (1995)	Bright UV continuum with P Cygni profile
1990, 1992	Parthasarathy et al. (1993; 1995)	Very bright emission lines dominates optical spectrum
1992-1994	Feibelman (1995)	Bright UV emission lines with no P Cygni profile
1996.3	Section 2.5	B=14.64, V=14.96 for central star alone
1994-2015	Sections 2.2, 2.3, & 2.4	V-band (i.e., [OIII] lines) fades steadily by 0.081 mag/year

Table 2. Stingray light curve 1889-2014

Julian Date	Year	Band	Magnitude	Sigma	Source
2411191.6463	1889.520	B	10.1	0.10	HCO (B 3743)
2411895.7797	1891.448	B	10.5	0.10	HCO (B 6263)
2411896.7927	1891.450	B	10.1	0.10	HCO (B 6284)
2412637.6167	1893.479	B	10.5	0.10	HCO (B 9644)
2412637.6247	1893.479	B	10.3	0.10	HCO (B 9645)
2412994.6657	1894.456	B	10.5	0.10	HCO (B 11416)
2413055.6143	1894.623	B	10.4	0.10	HCO (B 11901)
2413293.8362	1895.275	B	10.5	0.10	HCO (B 12968)
2413826.5242	1896.734	B	10.5	0.10	HCO (B 17442)
2414190.5163	1897.730	B	10.6	0.10	HCO (B 20488)
2414382.8107	1898.257	B	10.3	0.10	HCO (B 21140)
2414393.8365	1898.287	B	10.5	0.10	HCO (B 21222)
2414575.4898	1898.784	B	10.6	0.10	HCO (B 22027)
2414863.6364	1899.573	B	10.5	0.10	HCO (AM 22)
2414925.5190	1899.743	B	10.4	0.10	HCO (AM 162)
2414927.5695	1899.748	B	10.4	0.10	HCO (AM 173)
2415274.5747	1900.698	B	10.4	0.10	HCO (AM 644)
2415533.6520	1901.408	B	10.3	0.10	HCO (AM 816)
2415646.5346	1901.717	B	10.2	0.10	HCO (AM 1061)
2416011.5291	1902.716	B	10.2	0.10	HCO (AM 1545)
2416022.5612	1902.746	B	10.4	0.10	HCO (AM 1584)
2416297.6522	1903.499	B	10.2	0.10	HCO (AM 2084)
2416302.6630	1903.513	B	10.3	0.10	HCO (AM 2101)
2416311.5921	1903.538	B	10.2	0.10	HCO (AM 2128)
2416563.7676	1904.228	B	10.3	0.10	HCO (AM 2492)
2418102.5438	1908.441	B	10.4	0.10	HCO (AM 5549)
2418533.5118	1909.621	B	10.5	0.10	HCO (AM 6461)
2419239.5967	1911.554	B	10.6	0.10	HCO (AM 7589)
2420654.7449	1915.428	B	10.3	0.10	HCO (AM 10631)
2420720.5558	1915.609	B	10.3	0.10	HCO (AM 10972)
2421022.6793	1916.436	B	10.2	0.10	HCO (AM 11914)
2421081.5455	1916.597	B	10.3	0.10	HCO (AM 12308)
2421449.5399	1917.604	B	10.1	0.10	HCO (AM 13484)
2421757.6732	1918.448	B	10.2	0.10	HCO (AM 14060)
2422175.5687	1919.592	B	10.5	0.10	HCO (AM 14890)
2422542.5516	1920.597	B	10.6	0.10	HCO (AM 15379)
2423902.8720	1924.321	B	10.6	0.10	HCO (AX 484)
2423918.7837	1924.365	B	10.6	0.10	HCO (AX 527)
2423997.6383	1924.581	B	10.6	0.10	HCO (AX 732)
2424074.5172	1924.791	B	10.4	0.10	HCO (AX 862)
2424357.5954	1925.566	B	10.3	0.10	HCO (AX 1246)
2424433.5119	1925.774	B	10.3	0.10	HCO (AX 1364)
2424648.7057	1926.363	B	10.2	0.10	HCO (AX 1624)
2424670.6955	1926.424	B	10.3	0.10	HCO (AX 1675)
2425795.4167	1929.503	B	10.6	0.10	HCO (RB 426)
2425886.2442	1929.752	B	10.3	0.10	HCO (RB 569)

Table 2—Continued

Julian Date	Year	Band	Magnitude	Sigma	Source
2426189.4166	1930.582	B	10.5	0.10	HCO (RB 1198)
2426214.3066	1930.650	B	10.6	0.10	HCO (RB 1241)
2426505.4597	1931.447	B	10.6	0.10	HCO (RB 1855)
2426807.5668	1932.274	B	10.5	0.10	HCO (RB 2601)
2426812.5972	1932.288	B	10.5	0.10	HCO (RB 2623)
2426871.3811	1932.449	B	10.1	0.10	HCO (RB 2850)
2426939.2347	1932.634	B	10.3	0.10	HCO (RB 3351)
2427301.3199	1933.626	B	10.5	0.10	HCO (RB 4536)
2427601.4153	1934.447	B	10.5	0.10	HCO (RB 5311)
2427659.3741	1934.606	B	10.5	0.10	HCO (RB 5537)
2428049.2445	1935.673	B	10.8	0.10	HCO (RB 6389)
2428341.4863	1936.474	B	10.7	0.10	HCO (RB 6862)
2428448.2549	1936.766	B	10.7	0.10	HCO (RB 7124)
2428818.2554	1937.779	B	10.6	0.10	HCO (RB 7621)
2429130.3246	1938.633	B	10.8	0.10	HCO (RB 8177)
2429553.2404	1939.791	B	10.6	0.10	HCO (RB 9185)
2429746.4462	1940.320	B	10.7	0.10	HCO (RB 9531)
2429911.2340	1940.771	B	10.5	0.10	HCO (RB 10034)
2430150.3369	1941.426	B	10.6	0.10	HCO (RB 10750)
2430455.6135	1942.262	B	10.6	0.10	HCO (RB 11406)
2430963.2405	1943.652	B	10.6	0.10	HCO (RB 12357)
2431251.5632	1944.441	B	10.7	0.10	HCO (RB 12897)
2431262.5470	1944.471	B	10.6	0.10	HCO (RB 12923)
2431627.3593	1945.470	B	10.6	0.10	HCO (RB 13738)
2431993.5103	1946.472	B	10.5	0.10	HCO (RB 14474)
2432051.3238	1946.631	B	10.6	0.10	HCO (RB 14677)
2432353.4886	1947.458	B	10.7	0.10	HCO (RB 15162)
2432787.3021	1948.646	B	10.7	0.10	HCO (RB 15853)
2433512.3271	1950.631	B	10.7	0.10	HCO (RB 16747)
2433566.2594	1950.778	B	10.7	0.10	HCO (RB 16799)
2440200	1968.939	U	9.84	0.03	Hill et al. (1974)
2440200	1968.939	B	10.73	0.03	Hill et al. (1974)
2440200	1968.939	V	10.75	0.03	Hill et al. (1974)
2440739.4498	1970.417	B	10.7	0.10	HCO (DSB 38)
2440741.4428	1970.423	B	10.8	0.10	HCO (DSB 45)
2440773.3530	1970.510	B	10.8	0.10	HCO (DSB 73)
2440805.2599	1970.598	B	10.6	0.10	HCO (DSB 104)
2441148.3256	1971.537	B	10.7	0.10	HCO (DSB 257)
2441160.3084	1971.570	B	10.6	0.10	HCO (DSB 277)
2441538.2577	1972.604	B	10.9	0.10	HCO (DSB 377)
2441539.2500	1972.607	B	10.8	0.10	HCO (DSB 379)
2441540.2471	1972.610	B	10.6	0.10	HCO (DSB 381)
2443612.7774	1978.284	B	11.1	0.10	HCO (DSB 486)
2443691.6038	1978.500	B	11.0	0.10	HCO (DSB 524)
2444018.6753	1979.395	B	11.0	0.10	HCO (DSB 579)
2444024.7914	1979.412	B	11.0	0.10	HCO (DSB 618)

Table 2—Continued

Julian Date	Year	Band	Magnitude	Sigma	Source
2444163.5616	1979.792	B	11.0	0.10	HCO (DSB 634)
2444422	1980.498	U	9.95	0.02	Kozok (1985a)
2444422	1980.498	B	10.84	0.02	Kozok (1985a)
2444422	1980.498	V	10.88	0.01	Kozok (1985a)
2444431	1980.523	U	10.03	0.02	Kozok (1985a)
2444431	1980.523	B	10.92	0.02	Kozok (1985a)
2444431	1980.523	V	10.97	0.01	Kozok (1985a)
2444432	1980.526	U	10.08	0.02	Kozok (1985a)
2444432	1980.526	B	10.96	0.02	Kozok (1985a)
2444432	1980.526	V	10.99	0.01	Kozok (1985a)
2444697.1106	1981.253	B	10.8	0.10	HCO (DSB 723)
2444840.8754	1981.646	B	11.0	0.10	HCO (DSB 774)
2444843.8578	1981.655	B	11.0	0.10	HCO (DSB 775)
2445107.0202	1982.375	B	11.0	0.10	HCO (DSB 885)
2445134.9450	1982.452	B	10.9	0.10	HCO (DSB 896)
2445192.9166	1982.610	B	11.3	0.10	HCO (DSB 937)
2445520.9565	1983.508	B	11.6	0.10	HCO (DSB 1076)
2445819.9958	1984.327	B	11.7	0.10	HCO (DSB 1289)
2445960.8634	1984.713	B	11.8	0.10	HCO (DSB 1462)
2446145.1235	1985.217	B	12.1	0.10	HCO (DSB 1582)
2446319.8629	1985.696	B	12.3	0.10	HCO (DSB 1769)
2446348.8717	1985.775	B	12.3	0.10	HCO (DSB 1812)
2446695.8599	1986.725	B	12.3	0.10	HCO (DSB 2060)
2447019.8700	1987.612	B	12.2	0.10	HCO (DSB 2331)
2447356.9576	1988.535	B	12.5	0.10	HCO (DSB 2634)
2447413.9359	1988.691	B	12.3	0.10	HCO (DSB 2694)
2447682.1206	1989.425	B	12.3	0.10	HCO (DSB 2832)
2447760.9248	1989.641	B	12.3	0.10	HCO (DSB 2866)
2449418.1600	1994.178	V	11.3	0.15	Jones
2449419.1800	1994.181	V	10.7	0.15	Jones
2449420.1800	1994.184	V	10.5	0.15	Jones
2449421.1400	1994.187	V	10.7	0.15	Jones
2449422.2000	1994.189	V	10.7	0.15	Jones
2449424.1600	1994.195	V	10.7	0.15	Jones
2449428.1700	1994.206	V	10.7	0.15	Jones
2449432.1800	1994.217	V	10.8	0.15	Jones
2449433.2000	1994.220	V	10.7	0.15	Jones
2449435.1900	1994.225	V	10.7	0.15	Jones
2449438.1900	1994.233	V	10.8	0.15	Jones
2449447.2000	1994.258	V	10.7	0.15	Jones
2449452.9600	1994.274	V	10.5	0.15	Jones
2449453.9500	1994.276	V	10.7	0.15	Jones
2449472.8800	1994.328	V	11.1	0.15	Jones
2449476.9400	1994.339	V	10.7	0.15	Jones
2449482.9000	1994.356	V	10.8	0.15	Jones
2449487.8600	1994.369	V	11.3	0.15	Jones

Table 2—Continued

Julian Date	Year	Band	Magnitude	Sigma	Source
2449488.9200	1994.372	V	11.3	0.15	Jones
2449503.9300	1994.413	V	10.9	0.15	Jones
2449505.9100	1994.419	V	11.1	0.15	Jones
2449510.9100	1994.432	V	11.0	0.15	Jones
2449522.8300	1994.465	V	10.8	0.15	Jones
2449539.9100	1994.512	V	10.7	0.15	Jones
2449576.9800	1994.613	V	10.6	0.15	Jones
2449591.8700	1994.654	V	10.8	0.15	Jones
2449651.8800	1994.818	V	11.3	0.15	Jones
2449858.9000	1995.385	V	11.2	0.15	Jones
2449953.9200	1995.645	V	11.0	0.15	Jones
2450148.34	1996.176	B	14.64	0.05	Reindl et al. (2014)
2450148.34	1996.176	V	14.96	0.05	Reindl et al. (2014)
2450150.85	1996.183	V	15.4	0.05	Bobrowski (1998)
2450191.1700	1996.295	V	10.8	0.15	Jones
2450248.9200	1996.453	V	10.6	0.15	Jones
2450318.8800	1996.644	V	10.8	0.15	Jones
2451058.8600	1998.670	V	11.0	0.15	Jones
2451064.8760	1998.687	V	10.9	0.15	Jones
2451066.9500	1998.693	V	11.2	0.15	Jones
2451068.8980	1998.698	V	11.1	0.15	Jones
2451075.9480	1998.717	V	11.1	0.15	Jones
2451078.9060	1998.725	V	11.1	0.15	Jones
2451102.9260	1998.791	V	11.1	0.15	Jones
2451110.9300	1998.813	V	11.1	0.15	Jones
2451125.8900	1998.854	V	11.0	0.15	Jones
2451132.9090	1998.873	V	10.9	0.15	Jones
2451144.9000	1998.906	V	11.1	0.15	Jones
2451198.1390	1999.052	V	11.1	0.15	Jones
2451220.1590	1999.112	V	11.3	0.15	Jones
2451238.1620	1999.161	V	10.9	0.15	Jones
2451259.1950	1999.219	V	10.9	0.15	Jones
2451278.9660	1999.273	V	11.1	0.15	Jones
2451288.9310	1999.300	V	11.0	0.15	Jones
2451305.9060	1999.347	V	11.1	0.15	Jones
2451317.9130	1999.380	V	10.9	0.15	Jones
2451325.2240	1999.400	V	11.1	0.15	Jones
2451336.9530	1999.432	V	11.2	0.15	Jones
2451348.9690	1999.465	V	11.1	0.15	Jones
2451366.1980	1999.512	V	11.1	0.15	Jones
2451369.2220	1999.520	V	11.1	0.15	Jones
2451373.9570	1999.533	V	11.4	0.15	Jones
2451379.9320	1999.549	V	11.1	0.15	Jones
2451390.8930	1999.579	V	11.1	0.15	Jones
2451403.9040	1999.615	V	11.2	0.15	Jones
2451408.9580	1999.629	V	11.1	0.15	Jones

Table 2—Continued

Julian Date	Year	Band	Magnitude	Sigma	Source
2451428.9310	1999.684	V	11.1	0.15	Jones
2451448.8670	1999.738	V	11.1	0.15	Jones
2451463.9210	1999.779	V	11.1	0.15	Jones
2451465.9040	1999.785	V	11.1	0.15	Jones
2451470.8850	1999.798	V	11.1	0.15	Jones
2451496.8830	1999.870	V	11.1	0.15	Jones
2451557.1350	2000.035	V	11.1	0.15	Jones
2451561.1470	2000.046	V	11.1	0.15	Jones
2451571.1410	2000.073	V	11.2	0.15	Jones
2451583.1150	2000.106	V	11.2	0.15	Jones
2451603.1580	2000.161	V	11.1	0.15	Jones
2451612.1080	2000.185	V	11.2	0.15	Jones
2451618.1650	2000.202	V	11.1	0.15	Jones
2451666.9090	2000.335	V	11.1	0.15	Jones
2451689.2530	2000.396	V	11.1	0.15	Jones
2451703.2210	2000.435	V	11.1	0.15	Jones
2451730.8950	2000.510	V	11.1	0.15	Jones
2451757.8490	2000.584	V	11.2	0.15	Jones
2451762.8910	2000.598	V	11.5	0.15	Jones
2451850.8910	2000.839	V	11.2	0.15	Jones
2451869.9100	2000.891	V	11.1	0.15	Jones
2451939.8804	2001.082	V	11.66	0.22	ASAS
2451946.8850	2001.102	V	11.38	0.22	ASAS
2451949.8658	2001.110	V	11.78	0.22	ASAS
2451953.8386	2001.121	V	11.40	0.22	ASAS
2451955.8488	2001.126	V	11.61	0.22	ASAS
2451976.1650	2001.182	V	11.2	0.15	Jones
2451980.8003	2001.195	V	11.52	0.22	ASAS
2452025.7054	2001.317	V	11.67	0.22	ASAS
2452025.7094	2001.317	V	11.33	0.22	ASAS
2452026.7397	2001.320	V	11.30	0.22	ASAS
2452027.7596	2001.323	V	11.28	0.22	ASAS
2452030.7248	2001.331	V	11.58	0.22	ASAS
2452030.7511	2001.331	V	11.21	0.22	ASAS
2452031.7373	2001.334	V	11.38	0.22	ASAS
2452032.7199	2001.337	V	11.24	0.22	ASAS
2452033.7096	2001.339	V	11.36	0.22	ASAS
2452037.6818	2001.350	V	11.24	0.22	ASAS
2452037.7008	2001.350	V	11.41	0.22	ASAS
2452040.7062	2001.359	V	11.37	0.22	ASAS
2452052.6794	2001.391	V	11.36	0.22	ASAS
2452054.6889	2001.397	V	11.44	0.22	ASAS
2452055.6733	2001.400	V	11.34	0.22	ASAS
2452055.6939	2001.400	V	11.31	0.22	ASAS
2452055.9390	2001.400	V	10.9	0.15	Jones
2452056.6745	2001.402	V	11.41	0.22	ASAS

Table 2—Continued

Julian Date	Year	Band	Magnitude	Sigma	Source
2452056.6951	2001.402	V	11.42	0.22	ASAS
2452057.6703	2001.405	V	11.22	0.22	ASAS
2452058.6901	2001.408	V	11.38	0.22	ASAS
2452067.6349	2001.432	V	11.48	0.22	ASAS
2452068.6512	2001.435	V	11.50	0.22	ASAS
2452069.6673	2001.438	V	11.54	0.22	ASAS
2452070.6599	2001.441	V	11.28	0.22	ASAS
2452080.5344	2001.468	V	11.36	0.22	ASAS
2452081.6372	2001.471	V	11.61	0.22	ASAS
2452082.6507	2001.473	V	11.43	0.22	ASAS
2452083.6327	2001.476	V	11.36	0.22	ASAS
2452085.6257	2001.482	V	11.41	0.22	ASAS
2452086.6108	2001.484	V	11.55	0.22	ASAS
2452086.6316	2001.484	V	11.55	0.22	ASAS
2452086.8530	2001.485	V	10.9	0.15	Jones
2452087.6062	2001.487	V	11.33	0.22	ASAS
2452088.6049	2001.490	V	11.42	0.22	ASAS
2452088.6235	2001.490	V	11.43	0.22	ASAS
2452093.5358	2001.503	V	11.35	0.22	ASAS
2452094.5729	2001.506	V	11.36	0.22	ASAS
2452094.5842	2001.506	V	11.49	0.22	ASAS
2452103.5795	2001.531	V	11.27	0.22	ASAS
2452103.5959	2001.531	V	11.49	0.22	ASAS
2452104.5816	2001.533	V	11.33	0.22	ASAS
2452105.5882	2001.536	V	11.36	0.22	ASAS
2452115.5335	2001.563	V	11.80	0.22	ASAS
2452122.1720	2001.582	V	11.1	0.15	Jones
2452124.5178	2001.588	V	11.37	0.22	ASAS
2452125.5343	2001.591	V	11.35	0.22	ASAS
2452131.4906	2001.607	V	11.38	0.22	ASAS
2452135.5000	2001.618	V	11.36	0.22	ASAS
2452140.4924	2001.632	V	11.43	0.22	ASAS
2452142.5206	2001.637	V	11.31	0.22	ASAS
2452144.4891	2001.643	V	11.47	0.22	ASAS
2452151.4906	2001.662	V	11.52	0.22	ASAS
2452156.4760	2001.675	V	11.79	0.22	ASAS
2452164.4984	2001.697	V	11.53	0.22	ASAS
2452167.4762	2001.706	V	12.01	0.22	ASAS
2452168.5447	2001.709	V	11.65	0.22	ASAS
2452170.9569	2001.715	V	10.9	0.15	Jones
2452172.4844	2001.719	V	11.73	0.22	ASAS
2452180.5243	2001.741	V	11.57	0.22	ASAS
2452184.5221	2001.752	V	11.81	0.22	ASAS
2452191.5163	2001.771	V	11.62	0.22	ASAS
2452195.4854	2001.782	V	11.11	0.22	ASAS
2452197.4924	2001.788	V	11.94	0.22	ASAS

Table 2—Continued

Julian Date	Year	Band	Magnitude	Sigma	Source
2452198.5096	2001.791	V	11.61	0.22	ASAS
2452203.4956	2001.804	V	11.65	0.22	ASAS
2452203.5043	2001.804	V	11.77	0.22	ASAS
2452205.5173	2001.810	V	11.60	0.22	ASAS
2452302.1465	2002.074	V	11.2	0.15	Jones
2452309.1167	2002.093	V	11.5	0.15	Jones
2452320.1153	2002.124	V	11.2	0.15	Jones
2452359.1382	2002.230	V	11.2	0.15	Jones
2452368.9403	2002.257	V	11.2	0.15	Jones
2452428.9417	2002.421	V	11.2	0.15	Jones
2452505.9208	2002.632	V	11.1	0.15	Jones
2452510.6398	2002.645	V	11.61	0.22	ASAS
2452526.5885	2002.689	V	11.79	0.22	ASAS
2452535.5610	2002.713	V	11.56	0.22	ASAS
2452540.6191	2002.727	V	12.15	0.22	ASAS
2452545.5895	2002.741	V	11.54	0.22	ASAS
2452549.5558	2002.752	V	11.48	0.22	ASAS
2452559.5464	2002.779	V	11.59	0.22	ASAS
2452560.5584	2002.782	V	11.64	0.22	ASAS
2452561.5578	2002.785	V	11.65	0.22	ASAS
2452563.5373	2002.790	V	11.62	0.22	ASAS
2452565.5198	2002.795	V	11.65	0.22	ASAS
2452566.5385	2002.798	V	11.89	0.22	ASAS
2452660.8594	2003.056	V	11.48	0.22	ASAS
2452663.8687	2003.065	V	11.53	0.22	ASAS
2452671.8520	2003.087	V	11.66	0.22	ASAS
2452671.8520	2003.087	V	11.95	0.22	ASAS
2452678.1431	2003.104	V	11.4	0.15	Jones
2452678.8486	2003.106	V	11.82	0.22	ASAS
2452678.8716	2003.106	V	11.67	0.22	ASAS
2452685.8505	2003.125	V	11.66	0.22	ASAS
2452688.8499	2003.133	V	11.58	0.22	ASAS
2452703.8489	2003.174	V	11.22	0.22	ASAS
2452709.8384	2003.191	V	11.62	0.22	ASAS
2452711.8482	2003.196	V	11.66	0.22	ASAS
2452719.8236	2003.218	V	11.83	0.22	ASAS
2452719.8374	2003.218	V	11.38	0.22	ASAS
2452725.8025	2003.234	V	11.82	0.22	ASAS
2452727.8347	2003.240	V	11.21	0.22	ASAS
2452736.7614	2003.264	V	12.06	0.22	ASAS
2452747.8730	2003.295	V	11.31	0.22	ASAS
2452750.8662	2003.303	V	11.61	0.22	ASAS
2452751.7141	2003.305	V	11.84	0.22	ASAS
2452759.7983	2003.327	V	11.47	0.22	ASAS
2452770.8889	2003.358	V	11.3	0.15	Jones
2452784.6988	2003.395	V	11.75	0.22	ASAS

Table 2—Continued

Julian Date	Year	Band	Magnitude	Sigma	Source
2452787.7900	2003.404	V	11.60	0.22	ASAS
2452790.9107	2003.412	V	11.88	0.22	ASAS
2452790.9107	2003.412	V	11.69	0.22	ASAS
2452791.6407	2003.414	V	11.69	0.22	ASAS
2452802.8354	2003.445	V	11.40	0.22	ASAS
2452805.8355	2003.453	V	11.39	0.22	ASAS
2452812.2333	2003.471	V	11.3	0.15	Jones
2452820.6991	2003.494	V	11.69	0.22	ASAS
2452844.8257	2003.560	V	11.3	0.15	Jones
2452851.7313	2003.579	V	11.40	0.22	ASAS
2452865.7480	2003.617	V	11.73	0.22	ASAS
2452867.6999	2003.623	V	11.82	0.22	ASAS
2452876.6294	2003.647	V	11.64	0.22	ASAS
2452883.5493	2003.666	V	11.71	0.22	ASAS
2452885.5371	2003.672	V	11.64	0.22	ASAS
2452886.6790	2003.675	V	11.77	0.22	ASAS
2452893.5181	2003.693	V	11.88	0.22	ASAS
2452894.6070	2003.696	V	11.61	0.22	ASAS
2452906.6079	2003.729	V	11.57	0.22	ASAS
2452910.4864	2003.740	V	11.74	0.22	ASAS
2452912.5141	2003.745	V	11.62	0.22	ASAS
2452915.5404	2003.754	V	12.01	0.22	ASAS
2452917.5660	2003.759	V	11.67	0.22	ASAS
2452921.5653	2003.770	V	11.89	0.22	ASAS
2452923.5627	2003.776	V	11.94	0.22	ASAS
2452927.5127	2003.786	V	11.90	0.22	ASAS
2452929.5257	2003.792	V	11.71	0.22	ASAS
2452931.5299	2003.797	V	11.89	0.22	ASAS
2452933.5338	2003.803	V	11.84	0.22	ASAS
2452935.5351	2003.808	V	11.80	0.22	ASAS
2452954.5032	2003.860	V	11.70	0.22	ASAS
2453052.8736	2004.130	V	11.90	0.22	ASAS
2453056.8464	2004.141	V	11.72	0.22	ASAS
2453060.8541	2004.152	V	11.99	0.22	ASAS
2453061.8946	2004.154	V	11.80	0.22	ASAS
2453064.8438	2004.162	V	11.61	0.22	ASAS
2453069.8637	2004.176	V	11.78	0.22	ASAS
2453071.8658	2004.182	V	11.72	0.22	ASAS
2453077.8512	2004.198	V	11.86	0.22	ASAS
2453080.8684	2004.206	V	11.67	0.22	ASAS
2453080.8782	2004.206	V	11.90	0.22	ASAS
2453085.9064	2004.220	V	11.69	0.22	ASAS
2453091.8268	2004.236	V	11.72	0.22	ASAS
2453096.8798	2004.250	V	11.81	0.22	ASAS
2453098.8592	2004.256	V	12.02	0.22	ASAS
2453099.8203	2004.258	V	12.06	0.22	ASAS

Table 2—Continued

Julian Date	Year	Band	Magnitude	Sigma	Source
2453109.7758	2004.285	V	11.82	0.22	ASAS
2453112.7640	2004.294	V	11.72	0.22	ASAS
2453114.8238	2004.299	V	11.83	0.22	ASAS
2453122.7609	2004.321	V	11.76	0.22	ASAS
2453126.7968	2004.332	V	11.69	0.22	ASAS
2453132.8082	2004.349	V	11.66	0.22	ASAS
2453160.7912	2004.425	V	11.90	0.22	ASAS
2453163.7740	2004.433	V	11.86	0.22	ASAS
2453165.8024	2004.439	V	11.99	0.22	ASAS
2453171.7415	2004.455	V	11.90	0.22	ASAS
2453175.7424	2004.466	V	11.95	0.22	ASAS
2453178.6073	2004.474	V	12.10	0.22	ASAS
2453180.7050	2004.480	V	11.95	0.22	ASAS
2453187.5360	2004.498	V	11.52	0.22	ASAS
2453187.7002	2004.499	V	11.80	0.22	ASAS
2453189.7613	2004.504	V	11.58	0.22	ASAS
2453294.5414	2004.791	V	11.73	0.22	ASAS
2453398.8613	2005.077	V	12.10	0.22	ASAS
2453404.8696	2005.093	V	11.98	0.22	ASAS
2453408.8702	2005.104	V	12.12	0.22	ASAS
2453416.8635	2005.126	V	12.02	0.22	ASAS
2453420.8560	2005.137	V	11.90	0.22	ASAS
2453430.8633	2005.165	V	12.01	0.22	ASAS
2453436.8921	2005.181	V	11.66	0.22	ASAS
2453443.8497	2005.200	V	11.69	0.22	ASAS
2453446.8599	2005.208	V	11.73	0.22	ASAS
2453448.8490	2005.214	V	11.70	0.22	ASAS
2453448.8490	2005.214	V	12.16	0.22	ASAS
2453449.8600	2005.217	V	12.12	0.22	ASAS
2453452.8075	2005.225	V	11.79	0.22	ASAS
2453453.7784	2005.227	V	12.18	0.22	ASAS
2453455.8246	2005.233	V	11.85	0.22	ASAS
2453457.8797	2005.239	V	12.20	0.22	ASAS
2453462.8115	2005.252	V	11.87	0.22	ASAS
2453465.8270	2005.260	V	11.90	0.22	ASAS
2453468.8339	2005.269	V	11.92	0.22	ASAS
2453474.8106	2005.285	V	12.08	0.22	ASAS
2453477.7987	2005.293	V	12.30	0.22	ASAS
2453481.8177	2005.304	V	11.94	0.22	ASAS
2453487.7945	2005.320	V	11.90	0.22	ASAS
2453492.8215	2005.334	V	11.44	0.22	ASAS
2453496.8055	2005.345	V	11.98	0.22	ASAS
2453499.9028	2005.354	V	11.7	0.15	Jones
2453501.6721	2005.358	V	11.80	0.22	ASAS
2453502.8931	2005.362	V	11.8	0.15	Jones
2453503.9014	2005.365	V	12.2	0.15	Jones

Table 2—Continued

Julian Date	Year	Band	Magnitude	Sigma	Source
2453510.2403	2005.382	V	12.0	0.15	Jones
2453510.8345	2005.384	V	12.16	0.22	ASAS
2453512.7141	2005.389	V	11.95	0.22	ASAS
2453516.7668	2005.400	V	11.68	0.22	ASAS
2453520.7044	2005.411	V	12.30	0.22	ASAS
2453520.8889	2005.411	V	12.0	0.15	Jones
2453522.7321	2005.416	V	11.81	0.22	ASAS
2453524.7617	2005.422	V	12.51	0.22	ASAS
2453525.2313	2005.423	V	11.9	0.15	Jones
2453526.7830	2005.427	V	12.20	0.22	ASAS
2453527.8417	2005.430	V	12.2	0.15	Jones
2453528.8239	2005.433	V	12.01	0.22	ASAS
2453533.8521	2005.447	V	12.0	0.15	Jones
2453537.7329	2005.457	V	11.90	0.22	ASAS
2453544.7434	2005.476	V	12.32	0.22	ASAS
2453547.7901	2005.485	V	11.83	0.22	ASAS
2453548.8319	2005.488	V	12.1	0.15	Jones
2453551.7742	2005.496	V	12.37	0.22	ASAS
2453554.7389	2005.504	V	12.23	0.22	ASAS
2453556.8377	2005.509	V	12.10	0.22	ASAS
2453561.8375	2005.523	V	11.8	0.15	Jones
2453562.5703	2005.525	V	11.85	0.22	ASAS
2453564.6177	2005.531	V	12.02	0.22	ASAS
2453566.8306	2005.537	V	11.9	0.15	Jones
2453570.6111	2005.547	V	12.12	0.22	ASAS
2453573.6604	2005.556	V	12.03	0.22	ASAS
2453575.6783	2005.561	V	11.87	0.22	ASAS
2453583.5856	2005.583	V	11.99	0.22	ASAS
2453585.6427	2005.588	V	11.97	0.22	ASAS
2453587.6631	2005.594	V	11.94	0.22	ASAS
2453589.7100	2005.599	V	12.31	0.22	ASAS
2453592.5372	2005.607	V	12.03	0.22	ASAS
2453592.9396	2005.608	V	11.8	0.15	Jones
2453597.9118	2005.622	V	11.6	0.15	Jones
2453601.6689	2005.632	V	12.21	0.22	ASAS
2453603.6683	2005.638	V	12.00	0.22	ASAS
2453615.9000	2005.671	V	11.8	0.15	Jones
2453616.5523	2005.673	V	11.63	0.22	ASAS
2453620.6512	2005.684	V	11.90	0.22	ASAS
2453625.6121	2005.698	V	11.99	0.22	ASAS
2453631.5224	2005.714	V	12.30	0.22	ASAS
2453633.5429	2005.719	V	11.55	0.22	ASAS
2453637.9528	2005.732	V	11.5	0.15	Jones
2453639.5684	2005.736	V	11.97	0.22	ASAS
2453644.5947	2005.750	V	11.88	0.22	ASAS
2453648.5583	2005.761	V	11.95	0.22	ASAS

Table 2—Continued

Julian Date	Year	Band	Magnitude	Sigma	Source
2453650.5768	2005.766	V	11.89	0.22	ASAS
2453651.8847	2005.770	V	11.5	0.15	Jones
2453653.5248	2005.774	V	11.96	0.22	ASAS
2453658.5283	2005.788	V	12.05	0.22	ASAS
2453660.5531	2005.793	V	12.08	0.22	ASAS
2453665.5400	2005.807	V	12.15	0.22	ASAS
2453669.9035	2005.819	V	11.5	0.15	Jones
2453672.5139	2005.826	V	11.83	0.22	ASAS
2453675.5117	2005.834	V	11.30	0.22	ASAS
2453680.5014	2005.848	V	11.97	0.22	ASAS
2453693.8931	2005.885	V	11.5	0.15	Jones
2453759.8684	2006.065	V	12.12	0.22	ASAS
2453764.1389	2006.077	V	11.8	0.15	Jones
2453767.8726	2006.087	V	13.10	0.22	ASAS
2453774.8697	2006.106	V	12.12	0.22	ASAS
2453783.8886	2006.131	V	12.37	0.22	ASAS
2453790.8606	2006.150	V	12.08	0.22	ASAS
2453794.8718	2006.161	V	12.14	0.22	ASAS
2453797.8895	2006.169	V	12.07	0.22	ASAS
2453798.1688	2006.170	V	12.0	0.15	Jones
2453802.8748	2006.183	V	11.96	0.22	ASAS
2453806.8387	2006.194	V	11.66	0.22	ASAS
2453809.8700	2006.202	V	12.02	0.22	ASAS
2453813.8289	2006.213	V	11.84	0.22	ASAS
2453820.8212	2006.232	V	11.93	0.22	ASAS
2453820.8581	2006.232	V	12.07	0.22	ASAS
2453823.8838	2006.241	V	12.73	0.22	ASAS
2453829.8389	2006.257	V	12.17	0.22	ASAS
2453832.8288	2006.265	V	12.21	0.22	ASAS
2453835.8145	2006.273	V	11.98	0.22	ASAS
2453849.8533	2006.312	V	12.19	0.22	ASAS
2453852.7762	2006.320	V	11.90	0.22	ASAS
2453858.7578	2006.336	V	12.34	0.22	ASAS
2453858.7578	2006.336	V	12.03	0.22	ASAS
2453860.8193	2006.342	V	11.94	0.22	ASAS
2453860.9424	2006.342	V	11.8	0.15	Jones
2453864.7419	2006.352	V	12.37	0.22	ASAS
2453866.7336	2006.358	V	12.01	0.22	ASAS
2453871.7867	2006.372	V	11.89	0.22	ASAS
2453874.2285	2006.378	V	11.5	0.15	Jones
2453874.8760	2006.380	V	11.89	0.22	ASAS
2453880.7593	2006.396	V	11.96	0.22	ASAS
2453887.7141	2006.415	V	12.00	0.22	ASAS
2453891.9069	2006.427	V	11.8	0.15	Jones
2453893.7000	2006.432	V	11.75	0.22	ASAS
2453898.7406	2006.446	V	11.90	0.22	ASAS

Table 2—Continued

Julian Date	Year	Band	Magnitude	Sigma	Source
2453900.8053	2006.451	V	11.97	0.22	ASAS
2453902.7901	2006.457	V	12.46	0.22	ASAS
2453904.8119	2006.462	V	12.09	0.22	ASAS
2453906.8617	2006.468	V	12.13	0.22	ASAS
2453909.6979	2006.476	V	11.49	0.22	ASAS
2453910.8438	2006.479	V	12.0	0.15	Jones
2453913.7008	2006.487	V	12.60	0.22	ASAS
2453961.9479	2006.619	V	11.8	0.15	Jones
2453969.9382	2006.640	V	11.5	0.15	Jones
2453981.5070	2006.672	V	12.14	0.22	ASAS
2454006.8903	2006.742	V	11.7	0.15	Jones
2454028.9028	2006.802	V	11.5	0.15	Jones
2454133.8735	2007.089	V	12.12	0.22	ASAS
2454141.8739	2007.111	V	12.24	0.22	ASAS
2454145.8681	2007.122	V	12.31	0.22	ASAS
2454158.8794	2007.158	V	12.38	0.22	ASAS
2454162.8490	2007.169	V	12.33	0.22	ASAS
2454166.8473	2007.180	V	12.17	0.22	ASAS
2454176.8751	2007.207	V	12.56	0.22	ASAS
2454180.8332	2007.218	V	12.23	0.22	ASAS
2454187.8775	2007.237	V	12.09	0.22	ASAS
2454190.8382	2007.245	V	12.11	0.22	ASAS
2454193.8168	2007.253	V	11.93	0.22	ASAS
2454204.8726	2007.284	V	12.05	0.22	ASAS
2454208.8074	2007.294	V	12.14	0.22	ASAS
2454210.9472	2007.300	V	12.3	0.15	Jones
2454212.8477	2007.306	V	12.37	0.22	ASAS
2454230.7997	2007.355	V	12.03	0.22	ASAS
2454232.7736	2007.360	V	12.20	0.22	ASAS
2454232.8009	2007.360	V	12.35	0.22	ASAS
2454234.8409	2007.366	V	12.24	0.22	ASAS
2454245.6876	2007.395	V	12.30	0.22	ASAS
2454247.6793	2007.401	V	11.93	0.22	ASAS
2454253.8798	2007.418	V	11.95	0.22	ASAS
2454256.6701	2007.426	V	11.96	0.22	ASAS
2454258.7451	2007.431	V	11.99	0.22	ASAS
2454266.7835	2007.453	V	11.74	0.22	ASAS
2454272.6893	2007.469	V	11.96	0.22	ASAS
2454274.6799	2007.475	V	12.01	0.22	ASAS
2454277.6464	2007.483	V	11.92	0.22	ASAS
2454283.6649	2007.499	V	12.27	0.22	ASAS
2454284.8117	2007.503	V	12.68	0.22	ASAS
2454300.7397	2007.546	V	12.52	0.22	ASAS
2454302.7716	2007.552	V	12.12	0.22	ASAS
2454303.8236	2007.555	V	11.8	0.15	Jones
2454311.7078	2007.576	V	11.88	0.22	ASAS

Table 2—Continued

Julian Date	Year	Band	Magnitude	Sigma	Source
2454319.5581	2007.598	V	12.47	0.22	ASAS
2454329.5505	2007.625	V	12.06	0.22	ASAS
2454331.5490	2007.631	V	11.99	0.22	ASAS
2454336.5705	2007.644	V	12.22	0.22	ASAS
2454338.7201	2007.650	V	12.15	0.22	ASAS
2454341.5459	2007.658	V	12.04	0.22	ASAS
2454343.5567	2007.663	V	12.24	0.22	ASAS
2454353.6701	2007.691	V	11.99	0.22	ASAS
2454358.5176	2007.704	V	12.12	0.22	ASAS
2454360.5034	2007.710	V	12.65	0.22	ASAS
2454363.5142	2007.718	V	12.08	0.22	ASAS
2454365.5575	2007.724	V	11.88	0.22	ASAS
2454368.6116	2007.732	V	12.33	0.22	ASAS
2454376.5456	2007.754	V	12.46	0.22	ASAS
2454378.5402	2007.759	V	12.65	0.22	ASAS
2454378.5689	2007.759	V	12.56	0.22	ASAS
2454383.5520	2007.773	V	12.19	0.22	ASAS
2454392.5262	2007.797	V	11.96	0.22	ASAS
2454400.5187	2007.819	V	11.90	0.22	ASAS
2454407.5123	2007.839	V	12.58	0.22	ASAS
2454411.5069	2007.849	V	12.65	0.22	ASAS
2454502.8725	2008.100	V	12.44	0.22	ASAS
2454510.8659	2008.121	V	12.34	0.22	ASAS
2454517.8930	2008.141	V	11.92	0.22	ASAS
2454521.8572	2008.152	V	12.48	0.22	ASAS
2454524.8782	2008.160	V	12.16	0.22	ASAS
2454527.8753	2008.168	V	12.07	0.22	ASAS
2454531.8385	2008.179	V	12.34	0.22	ASAS
2454535.9008	2008.190	V	12.57	0.22	ASAS
2454543.8230	2008.212	V	12.32	0.22	ASAS
2454546.8327	2008.220	V	12.11	0.22	ASAS
2454555.7964	2008.244	V	12.50	0.22	ASAS
2454561.8265	2008.261	V	12.07	0.22	ASAS
2454564.8139	2008.269	V	12.47	0.22	ASAS
2454567.8049	2008.277	V	11.80	0.22	ASAS
2454570.7971	2008.286	V	12.34	0.22	ASAS
2454572.8470	2008.291	V	12.08	0.22	ASAS
2454576.8270	2008.302	V	12.46	0.22	ASAS
2454583.8015	2008.321	V	12.09	0.22	ASAS
2454589.7645	2008.337	V	12.20	0.22	ASAS
2454592.7407	2008.346	V	12.22	0.22	ASAS
2454594.8225	2008.351	V	12.05	0.22	ASAS
2454602.7343	2008.373	V	12.65	0.22	ASAS
2454606.7516	2008.384	V	12.79	0.22	ASAS
2454609.7037	2008.392	V	12.60	0.22	ASAS
2454617.7273	2008.414	V	11.88	0.22	ASAS

Table 2—Continued

Julian Date	Year	Band	Magnitude	Sigma	Source
2454623.7322	2008.430	V	12.47	0.22	ASAS
2454627.6957	2008.441	V	12.89	0.22	ASAS
2454629.6734	2008.447	V	12.15	0.22	ASAS
2454633.6629	2008.458	V	12.34	0.22	ASAS
2454638.7445	2008.472	V	12.33	0.22	ASAS
2454640.7113	2008.477	V	12.43	0.22	ASAS
2454642.6848	2008.482	V	12.21	0.22	ASAS
2454644.7043	2008.488	V	12.21	0.22	ASAS
2454646.7164	2008.493	V	12.52	0.22	ASAS
2454648.7597	2008.499	V	12.24	0.22	ASAS
2454650.8210	2008.505	V	12.44	0.22	ASAS
2454653.5883	2008.512	V	12.06	0.22	ASAS
2454655.6225	2008.518	V	12.62	0.22	ASAS
2454657.6614	2008.523	V	12.04	0.22	ASAS
2454660.6124	2008.531	V	12.36	0.22	ASAS
2454663.6202	2008.540	V	12.49	0.22	ASAS
2454664.7649	2008.543	V	12.44	0.22	ASAS
2454672.7114	2008.565	V	12.01	0.22	ASAS
2454681.6587	2008.589	V	12.27	0.22	ASAS
2454685.6391	2008.600	V	12.63	0.22	ASAS
2454687.5945	2008.605	V	12.12	0.22	ASAS
2454690.5458	2008.613	V	12.24	0.22	ASAS
2454701.6330	2008.644	V	12.92	0.22	ASAS
2454705.6663	2008.655	V	12.06	0.22	ASAS
2454710.6381	2008.668	V	12.10	0.22	ASAS
2454720.5595	2008.696	V	12.21	0.22	ASAS
2454728.5784	2008.718	V	12.07	0.22	ASAS
2454730.6178	2008.723	V	12.58	0.22	ASAS
2454733.6256	2008.731	V	13.12	0.22	ASAS
2454738.5167	2008.745	V	12.59	0.22	ASAS
2454741.5098	2008.753	V	12.06	0.22	ASAS
2454745.5096	2008.764	V	12.29	0.22	ASAS
2454747.5440	2008.769	V	12.48	0.22	ASAS
2454756.5339	2008.794	V	12.47	0.22	ASAS
2454759.5039	2008.802	V	12.72	0.22	ASAS
2454759.5257	2008.802	V	12.11	0.22	ASAS
2454762.5051	2008.810	V	12.31	0.22	ASAS
2454762.5246	2008.810	V	12.04	0.22	ASAS
2454765.5202	2008.819	V	12.41	0.22	ASAS
2454768.5156	2008.827	V	12.66	0.22	ASAS
2454772.4985	2008.838	V	12.52	0.22	ASAS
2454852.8693	2009.058	V	12.55	0.22	ASAS
2454869.8809	2009.104	V	13.09	0.22	ASAS
2454877.8747	2009.126	V	12.32	0.22	ASAS
2454882.8760	2009.140	V	12.67	0.22	ASAS
2454886.8588	2009.151	V	12.29	0.22	ASAS

Table 2—Continued

Julian Date	Year	Band	Magnitude	Sigma	Source
2454890.8723	2009.162	V	12.76	0.22	ASAS
2454904.8806	2009.200	V	12.59	0.22	ASAS
2454916.8113	2009.233	V	12.55	0.22	ASAS
2454924.9081	2009.255	V	12.13	0.22	ASAS
2454928.8875	2009.266	V	13.05	0.22	ASAS
2454937.7961	2009.290	V	12.81	0.22	ASAS
2454939.8639	2009.296	V	13.11	0.22	ASAS
2454946.7752	2009.315	V	12.33	0.22	ASAS
2454951.7892	2009.329	V	11.64	0.22	ASAS
2454954.7473	2009.337	V	12.27	0.22	ASAS
2454969.8717	2009.378	V	12.69	0.22	ASAS
2454975.7602	2009.394	V	12.37	0.22	ASAS
2454984.7423	2009.419	V	12.45	0.22	ASAS
2454988.7129	2009.430	V	12.96	0.22	ASAS
2455002.6908	2009.468	V	12.09	0.22	ASAS
2455006.6930	2009.479	V	12.18	0.22	ASAS
2455012.6958	2009.495	V	13.07	0.22	ASAS
2455014.6438	2009.501	V	12.34	0.22	ASAS
2455019.7041	2009.515	V	12.44	0.22	ASAS
2455021.7344	2009.520	V	12.56	0.22	ASAS
2455023.7397	2009.526	V	12.44	0.22	ASAS
2455040.5943	2009.572	V	12.16	0.22	ASAS
2455042.5812	2009.577	V	12.32	0.22	ASAS
2455067.6128	2009.646	V	12.30	0.22	ASAS
2455069.6101	2009.651	V	12.05	0.22	ASAS
2455075.6351	2009.668	V	12.09	0.22	ASAS
2455087.6403	2009.701	V	12.89	0.22	ASAS
2455092.6229	2009.714	V	12.06	0.22	ASAS
2455097.5133	2009.728	V	12.16	0.22	ASAS
2455099.5400	2009.733	V	12.70	0.22	ASAS
2455106.4991	2009.752	V	12.29	0.22	ASAS
2455111.5380	2009.766	V	12.48	0.22	ASAS
2455649.8986	2011.240	V	12.27	0.01	APASS
2455649.8992	2011.240	B	13.21	0.01	APASS
2455649.9001	2011.240	r'	12.22	0.01	APASS
2455649.9013	2011.240	i'	13.27	0.01	APASS
2455649.9020	2011.240	g'	12.31	0.01	APASS
2455677.6330	2011.316	V	12.28	0.01	APASS
2455677.6335	2011.316	B	13.21	0.01	APASS
2455677.6343	2011.316	r'	12.19	0.01	APASS
2455677.6356	2011.316	i'	13.22	0.01	APASS
2455677.6361	2011.316	g'	12.30	0.01	APASS
2456839.4923	2014.496	g'	12.52	0.01	DECam
2456839.4975	2014.496	r'	12.18	0.01	DECam
2456839.5027	2014.496	i'	13.35	0.01	DECam
2457104.9560	2015.224	V	12.63	0.01	Mount John

Table 2—Continued

Julian Date	Year	Band	Magnitude	Sigma	Source
2457104.9567	2015.224	V	12.65	0.01	Mount John
2457104.9573	2015.224	V	12.61	0.01	Mount John
2457104.9580	2015.224	V	12.65	0.01	Mount John
2457104.9593	2015.224	V	12.61	0.01	Mount John
2457104.9607	2015.224	V	12.59	0.01	Mount John
2457104.9613	2015.224	V	12.58	0.01	Mount John
2457104.9620	2015.224	V	12.62	0.01	Mount John
2457104.9707	2015.224	V	12.61	0.01	Mount John
2457104.9714	2015.224	V	12.61	0.01	Mount John
2457104.9720	2015.224	V	12.61	0.01	Mount John
2457104.9727	2015.224	V	12.64	0.01	Mount John
2457104.9734	2015.224	V	12.63	0.01	Mount John
2457104.9741	2015.224	V	12.62	0.01	Mount John
2457104.9747	2015.224	V	12.63	0.01	Mount John
2457104.9761	2015.224	V	12.61	0.01	Mount John
2457104.9767	2015.224	V	12.60	0.01	Mount John
2457104.9774	2015.224	V	12.60	0.01	Mount John
2457104.9781	2015.224	V	12.60	0.01	Mount John
2457104.9787	2015.224	V	12.61	0.01	Mount John
2457104.9794	2015.224	V	12.63	0.01	Mount John
2457104.9800	2015.224	V	12.61	0.01	Mount John
2457104.9807	2015.224	V	12.61	0.01	Mount John
2457104.9814	2015.224	V	12.59	0.01	Mount John
2457104.9821	2015.224	V	12.62	0.01	Mount John
2457104.9827	2015.224	V	12.60	0.01	Mount John
2457104.9834	2015.224	V	12.59	0.01	Mount John
2457104.9841	2015.224	V	12.60	0.01	Mount John
2457104.9847	2015.224	V	12.61	0.01	Mount John
2457104.9854	2015.224	V	12.61	0.01	Mount John
2457104.9860	2015.224	V	12.61	0.01	Mount John
2457104.9867	2015.224	V	12.62	0.01	Mount John
2457104.9874	2015.224	V	12.61	0.01	Mount John
2457104.9881	2015.224	V	12.58	0.01	Mount John
2457104.9887	2015.224	V	12.59	0.01	Mount John
2457104.9914	2015.224	V	12.59	0.01	Mount John
2457104.9921	2015.224	V	12.62	0.01	Mount John
2457104.9928	2015.224	V	12.60	0.01	Mount John
2457104.9934	2015.224	V	12.62	0.01	Mount John
2457104.9941	2015.224	V	12.63	0.01	Mount John
2457104.9948	2015.224	V	12.60	0.01	Mount John
2457104.9955	2015.224	V	12.61	0.01	Mount John
2457104.9961	2015.224	V	12.61	0.01	Mount John
2457104.9968	2015.224	V	12.62	0.01	Mount John
2457104.9974	2015.224	V	12.64	0.01	Mount John
2457104.9981	2015.224	V	12.61	0.01	Mount John
2457104.9988	2015.224	V	12.61	0.01	Mount John

Table 2—Continued

Julian Date	Year	Band	Magnitude	Sigma	Source
2457104.9994	2015.224	V	12.61	0.01	Mount John
2457105.0001	2015.224	V	12.62	0.01	Mount John
2457105.0008	2015.224	V	12.63	0.01	Mount John
2457105.0014	2015.224	V	12.64	0.01	Mount John
2457105.0021	2015.224	V	12.62	0.01	Mount John
2457105.0028	2015.224	V	12.60	0.01	Mount John
2457105.0034	2015.224	V	12.61	0.01	Mount John
2457105.0041	2015.224	V	12.62	0.01	Mount John
2457105.0048	2015.224	V	12.62	0.01	Mount John
2457105.0055	2015.224	V	12.62	0.01	Mount John
2457105.0061	2015.224	V	12.62	0.01	Mount John
2457105.0068	2015.224	V	12.61	0.01	Mount John
2457105.0075	2015.224	V	12.62	0.01	Mount John
2457105.0081	2015.224	V	12.65	0.01	Mount John
2457105.0088	2015.224	V	12.63	0.01	Mount John
2457105.0095	2015.224	V	12.62	0.01	Mount John
2457105.0101	2015.224	V	12.62	0.01	Mount John
2457105.0108	2015.224	V	12.62	0.01	Mount John
2457105.0115	2015.224	V	12.61	0.01	Mount John
2457105.0122	2015.224	V	12.63	0.01	Mount John
2457105.0128	2015.224	V	12.61	0.01	Mount John
2457105.0135	2015.224	V	12.60	0.01	Mount John
2457105.0141	2015.224	V	12.62	0.01	Mount John
2457105.0148	2015.224	V	12.62	0.01	Mount John
2457105.0155	2015.224	V	12.60	0.01	Mount John
2457105.0161	2015.224	V	12.62	0.01	Mount John
2457105.0169	2015.224	V	12.62	0.01	Mount John
2457105.0176	2015.224	V	12.62	0.01	Mount John
2457105.0182	2015.224	V	12.66	0.01	Mount John
2457105.0189	2015.224	V	12.62	0.01	Mount John
2457105.0196	2015.224	V	12.60	0.01	Mount John
2457105.0202	2015.224	V	12.62	0.01	Mount John
2457105.0209	2015.224	V	12.63	0.01	Mount John
2457105.0216	2015.224	V	12.62	0.01	Mount John
2457105.0222	2015.224	V	12.61	0.01	Mount John
2457105.0229	2015.224	V	12.62	0.01	Mount John
2457105.0236	2015.224	V	12.62	0.01	Mount John
2457105.0242	2015.224	V	12.62	0.01	Mount John
2457105.0249	2015.224	V	12.62	0.01	Mount John
2457105.0256	2015.224	V	12.60	0.01	Mount John
2457105.0262	2015.224	V	12.62	0.01	Mount John
2457105.0269	2015.224	V	12.63	0.01	Mount John
2457105.0276	2015.224	V	12.65	0.01	Mount John
2457105.0282	2015.224	V	12.59	0.01	Mount John
2457105.0289	2015.224	V	12.62	0.01	Mount John
2457105.0296	2015.224	V	12.63	0.01	Mount John

Table 2—Continued

Julian Date	Year	Band	Magnitude	Sigma	Source
2457105.0302	2015.224	V	12.63	0.01	Mount John
2457105.0309	2015.224	V	12.61	0.01	Mount John
2457105.0343	2015.224	V	12.63	0.01	Mount John
2457105.0349	2015.224	V	12.63	0.01	Mount John
2457105.0356	2015.224	V	12.62	0.01	Mount John
2457105.0363	2015.224	V	12.62	0.01	Mount John
2457105.0369	2015.224	V	12.62	0.01	Mount John
2457105.0376	2015.224	V	12.65	0.01	Mount John
2457105.0383	2015.224	V	12.63	0.01	Mount John
2457105.0389	2015.224	V	12.61	0.01	Mount John
2457105.0396	2015.224	V	12.64	0.01	Mount John
2457105.0403	2015.224	V	12.62	0.01	Mount John
2457105.0409	2015.224	V	12.62	0.01	Mount John
2457105.0416	2015.224	V	12.62	0.01	Mount John
2457105.0423	2015.224	V	12.64	0.01	Mount John
2457105.0430	2015.224	V	12.63	0.01	Mount John
2457105.0436	2015.224	V	12.63	0.01	Mount John
2457105.0443	2015.224	V	12.61	0.01	Mount John
2457105.0450	2015.224	V	12.62	0.01	Mount John
2457105.0456	2015.224	V	12.62	0.01	Mount John
2457105.0463	2015.224	V	12.62	0.01	Mount John
2457105.0469	2015.224	V	12.62	0.01	Mount John
2457105.0476	2015.224	V	12.61	0.01	Mount John
2457105.0483	2015.224	V	12.61	0.01	Mount John
2457105.0489	2015.224	V	12.60	0.01	Mount John
2457105.0496	2015.224	V	12.60	0.01	Mount John
2457105.0503	2015.224	V	12.62	0.01	Mount John
2457105.0509	2015.224	V	12.61	0.01	Mount John
2457105.0516	2015.224	V	12.63	0.01	Mount John
2457105.0523	2015.224	V	12.62	0.01	Mount John
2457105.0529	2015.224	V	12.64	0.01	Mount John
2457105.0536	2015.224	V	12.62	0.01	Mount John
2457105.0543	2015.224	V	12.63	0.01	Mount John
2457105.0549	2015.224	V	12.62	0.01	Mount John
2457105.0556	2015.224	V	12.63	0.01	Mount John
2457105.0563	2015.224	V	12.62	0.01	Mount John
2457105.0569	2015.224	V	12.61	0.01	Mount John
2457105.0576	2015.224	V	12.61	0.01	Mount John
2457105.0583	2015.224	V	12.62	0.01	Mount John
2457105.0589	2015.224	V	12.59	0.01	Mount John
2457105.0596	2015.224	V	12.60	0.01	Mount John
2457105.0603	2015.224	V	12.63	0.01	Mount John
2457105.0609	2015.224	V	12.61	0.01	Mount John
2457105.0616	2015.224	V	12.56	0.01	Mount John
2457105.0623	2015.224	V	12.61	0.01	Mount John
2457105.0629	2015.224	V	12.61	0.01	Mount John

Table 2—Continued

Julian Date	Year	Band	Magnitude	Sigma	Source
2457105.0636	2015.224	V	12.59	0.01	Mount John
2457105.0643	2015.224	V	12.61	0.01	Mount John
2457105.0650	2015.224	V	12.61	0.01	Mount John
2457105.0656	2015.224	V	12.62	0.01	Mount John
2457105.0663	2015.224	V	12.61	0.01	Mount John
2457105.0670	2015.224	V	12.62	0.01	Mount John
2457105.0676	2015.224	V	12.61	0.01	Mount John
2457105.0683	2015.224	V	12.60	0.01	Mount John
2457105.0690	2015.224	V	12.66	0.01	Mount John
2457105.0696	2015.224	V	12.61	0.01	Mount John
2457105.0703	2015.224	V	12.58	0.01	Mount John
2457105.0710	2015.224	V	12.61	0.01	Mount John
2457105.0717	2015.224	V	12.63	0.01	Mount John
2457105.0723	2015.224	V	12.62	0.01	Mount John
2457105.0730	2015.224	V	12.65	0.01	Mount John
2457105.0737	2015.224	V	12.63	0.01	Mount John
2457105.0743	2015.224	V	12.61	0.01	Mount John
2457105.0750	2015.224	V	12.65	0.01	Mount John
2457105.0757	2015.224	V	12.63	0.01	Mount John
2457105.0763	2015.224	V	12.60	0.01	Mount John
2457105.0770	2015.224	V	12.61	0.01	Mount John
2457105.0777	2015.224	V	12.63	0.01	Mount John
2457105.0784	2015.224	V	12.62	0.01	Mount John
2457105.0790	2015.224	V	12.63	0.01	Mount John
2457105.0797	2015.224	V	12.61	0.01	Mount John
2457105.0803	2015.224	V	12.60	0.01	Mount John
2457105.0810	2015.224	V	12.63	0.01	Mount John
2457105.0817	2015.224	V	12.61	0.01	Mount John
2457105.0823	2015.224	V	12.63	0.01	Mount John
2457105.0830	2015.224	V	12.62	0.01	Mount John
2457105.0837	2015.224	V	12.60	0.01	Mount John
2457105.0843	2015.224	V	12.62	0.01	Mount John
2457105.0850	2015.224	V	12.64	0.01	Mount John
2457105.0857	2015.224	V	12.63	0.01	Mount John
2457105.0863	2015.224	V	12.61	0.01	Mount John
2457105.0870	2015.224	V	12.60	0.01	Mount John
2457105.0877	2015.224	V	12.63	0.01	Mount John
2457107.9548	2015.232	V	12.57	0.01	Mount John
2457107.9554	2015.232	V	12.56	0.01	Mount John
2457107.9561	2015.232	V	12.58	0.01	Mount John
2457107.9568	2015.232	V	12.58	0.01	Mount John
2457107.9574	2015.232	V	12.56	0.01	Mount John
2457109.1266	2015.235	V	12.62	0.01	Mount John
2457109.1274	2015.235	V	12.60	0.01	Mount John
2457109.1281	2015.235	V	12.63	0.01	Mount John
2457109.1287	2015.235	V	12.59	0.01	Mount John

Table 2—Continued

Julian Date	Year	Band	Magnitude	Sigma	Source
2457109.1294	2015.235	V	12.61	0.01	Mount John
2457109.1301	2015.235	V	12.62	0.01	Mount John
2457109.1307	2015.235	V	12.61	0.01	Mount John
2457109.1314	2015.235	V	12.62	0.01	Mount John
2457109.1321	2015.235	V	12.61	0.01	Mount John
2457109.1327	2015.235	V	12.63	0.01	Mount John
2457109.1334	2015.235	V	12.56	0.01	Mount John
2457109.1341	2015.235	V	12.61	0.01	Mount John
2457109.1347	2015.235	V	12.60	0.01	Mount John
2457109.1354	2015.235	V	12.61	0.01	Mount John
2457109.1361	2015.235	V	12.62	0.01	Mount John
2457109.1368	2015.235	V	12.60	0.01	Mount John
2457109.1374	2015.235	V	12.60	0.01	Mount John
2457109.1381	2015.235	V	12.61	0.01	Mount John
2457109.1387	2015.235	V	12.62	0.01	Mount John
2457109.1394	2015.235	V	12.62	0.01	Mount John
2457109.1401	2015.235	V	12.61	0.01	Mount John
2457109.1407	2015.235	V	12.61	0.01	Mount John
2457109.1414	2015.235	V	12.59	0.01	Mount John
2457109.1421	2015.235	V	12.59	0.01	Mount John
2457109.1427	2015.235	V	12.61	0.01	Mount John
2457109.1434	2015.235	V	12.62	0.01	Mount John
2457109.1441	2015.235	V	12.61	0.01	Mount John
2457109.1447	2015.235	V	12.61	0.01	Mount John
2457109.1454	2015.235	V	12.60	0.01	Mount John
2457109.1461	2015.235	V	12.59	0.01	Mount John
2457109.1467	2015.235	V	12.60	0.01	Mount John
2457109.1474	2015.235	V	12.60	0.01	Mount John
2457109.1481	2015.235	V	12.61	0.01	Mount John
2457109.1487	2015.235	V	12.62	0.01	Mount John
2457109.1494	2015.235	V	12.61	0.01	Mount John
2457109.1501	2015.235	V	12.59	0.01	Mount John
2457109.1507	2015.235	V	12.62	0.01	Mount John
2457109.1514	2015.235	V	12.59	0.01	Mount John
2457109.1521	2015.235	V	12.61	0.01	Mount John
2457109.1527	2015.235	V	12.61	0.01	Mount John
2457109.1534	2015.235	V	12.61	0.01	Mount John
2457109.1541	2015.235	V	12.61	0.01	Mount John
2457109.1548	2015.235	V	12.61	0.01	Mount John
2457109.1554	2015.235	V	12.61	0.01	Mount John
2457109.1561	2015.235	V	12.59	0.01	Mount John
2457109.1567	2015.235	V	12.60	0.01	Mount John
2457109.1574	2015.235	V	12.60	0.01	Mount John
2457109.1581	2015.235	V	12.62	0.01	Mount John
2457109.1588	2015.235	V	12.62	0.01	Mount John
2457109.1594	2015.235	V	12.59	0.01	Mount John

Table 2—Continued

Julian Date	Year	Band	Magnitude	Sigma	Source
2457109.1601	2015.235	V	12.62	0.01	Mount John
2457109.1608	2015.235	V	12.62	0.01	Mount John
2457109.1621	2015.235	V	12.58	0.01	Mount John
2457109.1628	2015.235	V	12.60	0.01	Mount John
2457109.1634	2015.235	V	12.62	0.01	Mount John
2457109.1641	2015.235	V	12.62	0.01	Mount John
2457109.1648	2015.235	V	12.58	0.01	Mount John
2457109.1654	2015.235	V	12.61	0.01	Mount John
2457109.1661	2015.235	V	12.61	0.01	Mount John
2457109.1668	2015.235	V	12.61	0.01	Mount John
2457109.1674	2015.235	V	12.62	0.01	Mount John
2457109.1681	2015.235	V	12.62	0.01	Mount John
2457109.1688	2015.235	V	12.59	0.01	Mount John
2457109.1694	2015.235	V	12.61	0.01	Mount John
2457109.1701	2015.235	V	12.61	0.01	Mount John
2457109.1708	2015.235	V	12.59	0.01	Mount John
2457109.1715	2015.235	V	12.62	0.01	Mount John
2457109.1721	2015.235	V	12.61	0.01	Mount John
2457109.1728	2015.235	V	12.58	0.01	Mount John
2457109.1734	2015.235	V	12.61	0.01	Mount John
2457109.1741	2015.235	V	12.61	0.01	Mount John
2457109.1748	2015.235	V	12.62	0.01	Mount John
2457109.1754	2015.235	V	12.61	0.01	Mount John
2457109.1761	2015.235	V	12.60	0.01	Mount John
2457109.1768	2015.235	V	12.59	0.01	Mount John
2457109.1774	2015.235	V	12.61	0.01	Mount John
2457109.1781	2015.235	V	12.61	0.01	Mount John
2457109.1788	2015.235	V	12.59	0.01	Mount John
2457109.1794	2015.235	V	12.61	0.01	Mount John
2457109.1801	2015.235	V	12.61	0.01	Mount John
2457109.1808	2015.235	V	12.62	0.01	Mount John
2457109.1814	2015.235	V	12.60	0.01	Mount John
2457109.1821	2015.235	V	12.61	0.01	Mount John
2457109.1828	2015.235	V	12.57	0.01	Mount John
2457109.1834	2015.235	V	12.58	0.01	Mount John
2457109.1841	2015.235	V	12.62	0.01	Mount John
2457109.1848	2015.235	V	12.62	0.01	Mount John
2457109.1854	2015.235	V	12.61	0.01	Mount John
2457109.1861	2015.235	V	12.62	0.01	Mount John
2457109.1868	2015.235	V	12.63	0.01	Mount John
2457109.1874	2015.235	V	12.61	0.01	Mount John
2457109.1881	2015.235	V	12.63	0.01	Mount John
2457109.1888	2015.235	V	12.60	0.01	Mount John
2457109.1894	2015.235	V	12.61	0.01	Mount John
2457109.1901	2015.235	V	12.62	0.01	Mount John
2457109.1908	2015.235	V	12.61	0.01	Mount John

Table 2—Continued

Julian Date	Year	Band	Magnitude	Sigma	Source
2457109.1914	2015.235	V	12.61	0.01	Mount John
2457109.1921	2015.235	V	12.61	0.01	Mount John
2457109.1928	2015.235	V	12.61	0.01	Mount John
2457109.1934	2015.235	V	12.62	0.01	Mount John
2457109.1941	2015.235	V	12.61	0.01	Mount John
2457109.1948	2015.235	V	12.62	0.01	Mount John
2457109.1954	2015.235	V	12.61	0.01	Mount John
2457109.1961	2015.235	V	12.62	0.01	Mount John
2457109.1968	2015.235	V	12.61	0.01	Mount John
2457109.1975	2015.235	V	12.62	0.01	Mount John
2457109.1981	2015.235	V	12.61	0.01	Mount John
2457109.1988	2015.235	V	12.61	0.01	Mount John
2457109.1994	2015.235	V	12.58	0.01	Mount John
2457109.2001	2015.235	V	12.59	0.01	Mount John
2457109.2008	2015.235	V	12.61	0.01	Mount John
2457109.2014	2015.235	V	12.58	0.01	Mount John
2457109.2021	2015.235	V	12.61	0.01	Mount John
2457109.2028	2015.235	V	12.60	0.01	Mount John
2457109.2035	2015.235	V	12.59	0.01	Mount John
2457109.2041	2015.235	V	12.61	0.01	Mount John
2457109.2048	2015.235	V	12.62	0.01	Mount John
2457109.2054	2015.235	V	12.59	0.01	Mount John
2457109.2061	2015.235	V	12.61	0.01	Mount John
2457109.2068	2015.235	V	12.63	0.01	Mount John
2457109.2074	2015.235	V	12.62	0.01	Mount John
2457109.2081	2015.235	V	12.61	0.01	Mount John
2457109.2088	2015.235	V	12.61	0.01	Mount John
2457109.2094	2015.235	V	12.61	0.01	Mount John
2457109.2101	2015.235	V	12.60	0.01	Mount John
2457109.2107	2015.235	V	12.62	0.01	Mount John
2457109.2114	2015.235	V	12.61	0.01	Mount John
2457109.2121	2015.235	V	12.61	0.01	Mount John
2457109.2127	2015.235	V	12.61	0.01	Mount John
2457109.2134	2015.235	V	12.62	0.01	Mount John
2457109.2141	2015.235	V	12.61	0.01	Mount John
2457109.2147	2015.235	V	12.59	0.01	Mount John
2457109.2154	2015.235	V	12.60	0.01	Mount John
2457109.2161	2015.235	V	12.60	0.01	Mount John
2457109.2167	2015.235	V	12.58	0.01	Mount John
2457109.2174	2015.235	V	12.61	0.01	Mount John
2457109.2180	2015.235	V	12.62	0.01	Mount John
2457109.2187	2015.235	V	12.59	0.01	Mount John
2457109.2201	2015.235	V	12.61	0.01	Mount John
2457109.2207	2015.235	V	12.62	0.01	Mount John
2457109.2214	2015.235	V	12.62	0.01	Mount John
2457109.2221	2015.235	V	12.60	0.01	Mount John

Table 2—Continued

Julian Date	Year	Band	Magnitude	Sigma	Source
2457109.2227	2015.235	V	12.61	0.01	Mount John
2457109.2234	2015.235	V	12.63	0.01	Mount John
2457109.2240	2015.235	V	12.61	0.01	Mount John
2457109.2247	2015.235	V	12.61	0.01	Mount John
2457109.2254	2015.235	V	12.61	0.01	Mount John
2457109.2260	2015.235	V	12.59	0.01	Mount John
2457109.2267	2015.235	V	12.60	0.01	Mount John
2457109.2280	2015.235	V	12.57	0.01	Mount John
2457109.2287	2015.235	V	12.60	0.01	Mount John
2457109.2294	2015.235	V	12.61	0.01	Mount John
2457109.2300	2015.235	V	12.61	0.01	Mount John
2457109.2307	2015.235	V	12.59	0.01	Mount John
2457109.2314	2015.235	V	12.58	0.01	Mount John
2457109.2321	2015.235	V	12.63	0.01	Mount John
2457109.2327	2015.235	V	12.62	0.01	Mount John
2457109.2334	2015.235	V	12.62	0.01	Mount John
2457109.2341	2015.235	V	12.62	0.01	Mount John
2457109.2347	2015.235	V	12.59	0.01	Mount John
2457109.2354	2015.235	V	12.59	0.01	Mount John
2457109.2361	2015.235	V	12.60	0.01	Mount John
2457109.2367	2015.235	V	12.61	0.01	Mount John
2457109.2374	2015.235	V	12.61	0.01	Mount John
2457109.2381	2015.235	V	12.62	0.01	Mount John
2457109.2388	2015.235	V	12.58	0.01	Mount John
2457109.2394	2015.235	V	12.58	0.01	Mount John
2457109.2401	2015.235	V	12.60	0.01	Mount John
2457109.2408	2015.235	V	12.61	0.01	Mount John
2457109.2414	2015.235	V	12.60	0.01	Mount John
2457109.2414	2015.235	V	12.62	0.01	Mount John

Table 3. Stingray evolution

Year	$\text{Log}(T_{eff})$	$\text{Log}(L/L_{\odot})$
c. 1001	3.70 ± 0.20^a	3.74 ± 0.5^a
1889	4.48 ± 0.10^b	3.74 ± 0.41^e
1980	4.45 ± 0.11^c	3.38 ± 0.41^e
1988	4.58 ± 0.13^d	$2.65 \pm 0.75^{d,f}$
1996	4.70 ± 0.10^d	$2.73 \pm 0.67^{d,f}$
2002	4.78 ± 0.08^d	$2.24 \pm 0.63^{d,f}$
2006	4.74 ± 0.09^d	$2.09 \pm 0.65^{d,f}$

^aThe temperature and luminosity for the epoch of the ejection of the planetary nebula shell are simply meant to represent the approximate position of the central star when it leaves the AGB. The important realization is that the shell was ejected about a thousand years before the current situation, and this is greatly at odds with theoretical models that require an order of magnitude longer time, unless the central star is much more massive than anyone expects.

^bThe central star was typed as B0 around 1920.

^cThe central star was typed as B1 in 1971.

^dReindl et al. (2014).

^eThe luminosity is based on the observed B magnitudes (see Table 1), corrected for extinction (with $E(B - V) = 0.20 \pm 0.04$), corrected to V magnitudes (with the $B - V$ color appropriate for the observed spectral type), converted to absolute V magnitude (with a distance of 1.6 ± 0.6 kpc), corrected to the absolute bolometric magnitude (with a correction appropriate for the observed spectral type), and converted to luminosity in solar units (with a scaling from our Sun).

^fThe luminosity is calculated as $L = (\sigma T^4)(4\pi GM_{star}/g)$, where g is the star’s surface gravity as measured by Reindl et al. (2014), and where the mass of the central star is taken to be the reasonable middle value of $0.55 M_{\odot}$ (as appropriate for comparison with the evolution tracks of Schönberner 1983).

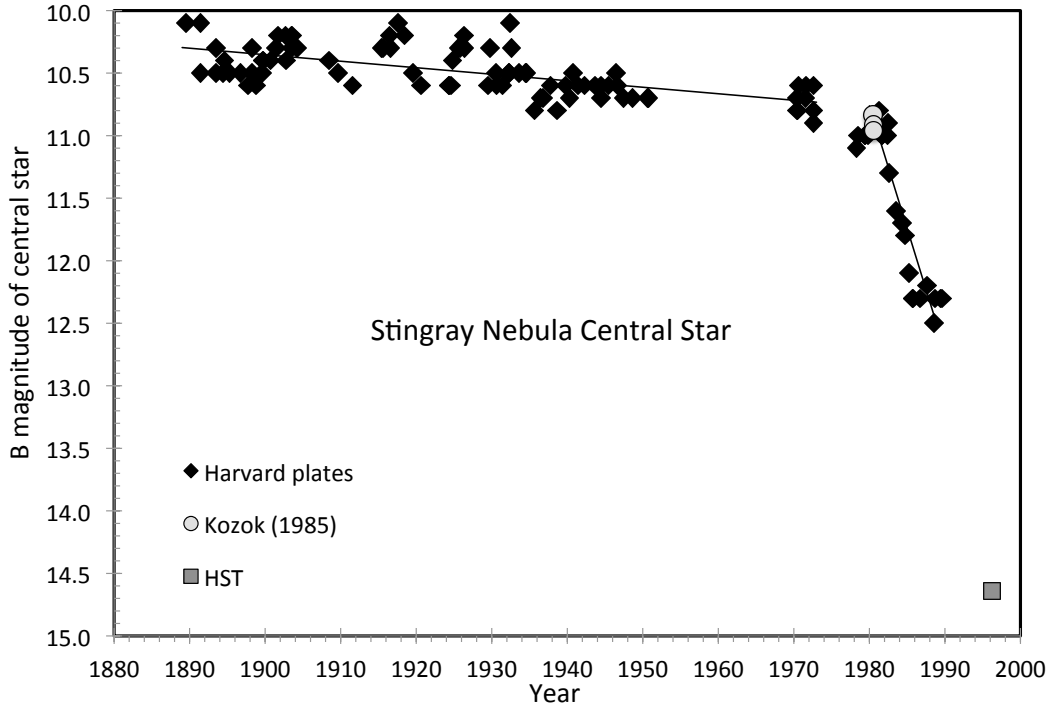


Fig. 1.— B-band light curve of the central star of the Stingray Nebula. The Harvard plates show a steady and significant decline from 1889 to 1980, followed by a sudden fast fading from 1980 to 1989. The average rate from 1889-1980 is 0.0051 mag/year, as represented by the thin line. So in some sense, the star knew to anticipate the upcoming ionization event in 1980. Superposed on this linear decline are apparent variations on the time scale of a decade by up to half a magnitude in amplitude. The B-band magnitudes from 1889-1980 are certainly of light from the photosphere of the central star, because the four spectra before 1980 show either no emission lines or very weak emission lines. In 1980, the three B-magnitudes from Kozok (1985a) confirm the Harvard light curve. After 1980, the B magnitude starts fading fast, with an apparent rate of 0.20 mag/year, as represented by the thin line. This huge dimming is likely caused by the observed decrease in the size of the central star, although detailed calculations do not reproduce the speed of the decline. If emission lines contributed significantly from 1980-1989, then this could only mean that the central star was fading even faster. In 1996, *HST* resolved the central star from the surrounding nebulosity, while the B-band flux was taken from a spectrum without any emission contribution, so this magnitude is also of the central star alone. The decline from 1980 to 1989 can be extrapolated to accurately reproduce the 1996 *HST* magnitude. Importantly, there is no sign of any brightening in the B-band light curve around the time of 1980, when the ultraviolet flux suddenly turned on very brightly.

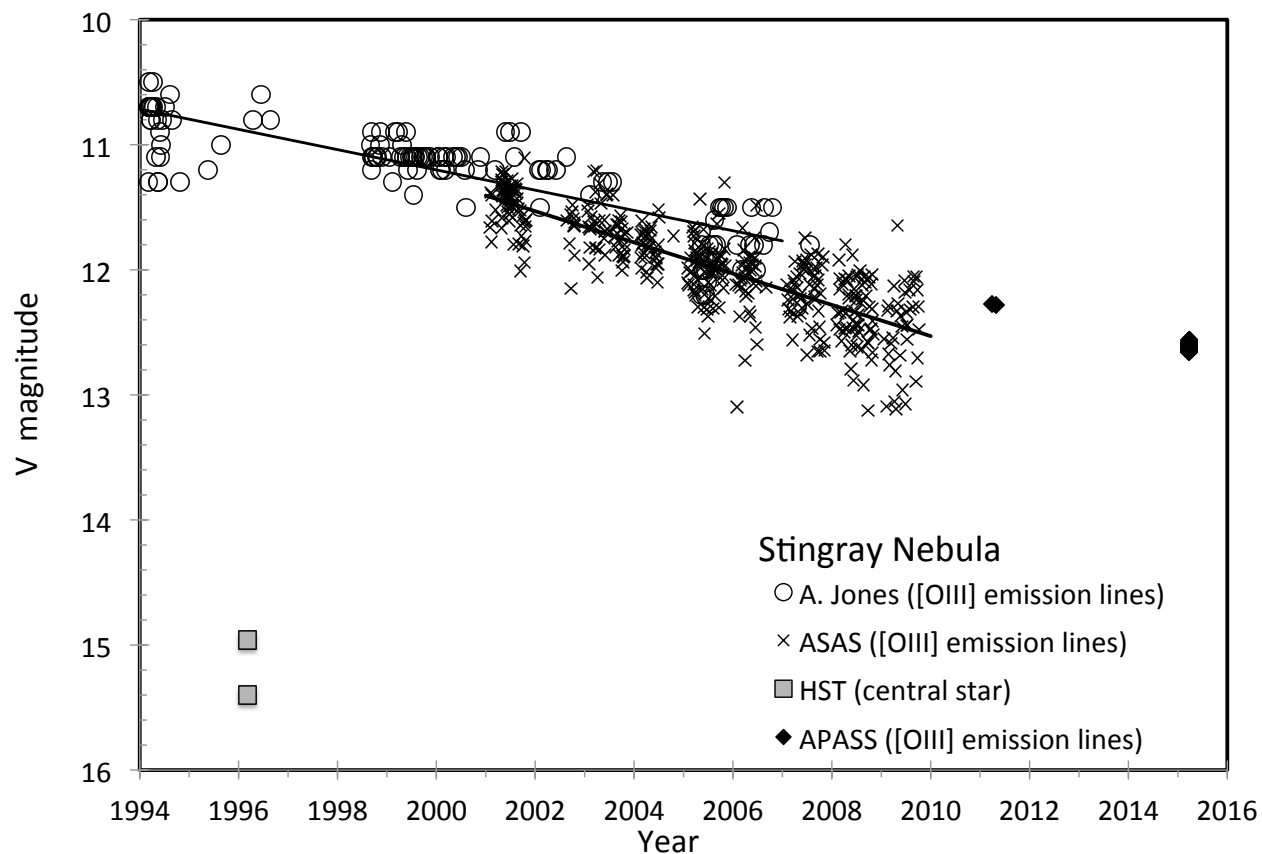


Fig. 2.— V-band light curve of the Stingray from 1994-2015. Albert Jones and *ASAS* have reported many V-band measures, and they are in reasonable agreement. (Small differences are expected between observers due to small differences in their spectral sensitivity in looking at an emission line source as compared to the continuum of the normal comparison stars.) They show a slow rate of decline (indicated by the thin lines), with rates of 0.081 mag/year and 0.125 mag/year. Importantly, these V-band magnitudes are really just measuring the brightness of the two [OIII] emission lines at 5007\AA and 4959\AA , because contemporaneous spectra show that these lines provide 98% of the detected light for the V-band. Also importantly, contemporaneous *HST* narrow-band images centered on the [OIII] lines shows that the central star is very faint. The V-band magnitude for the central star alone has been isolated with *HST* in 1996, with the star itself providing less than 2% of the overall V-band flux.

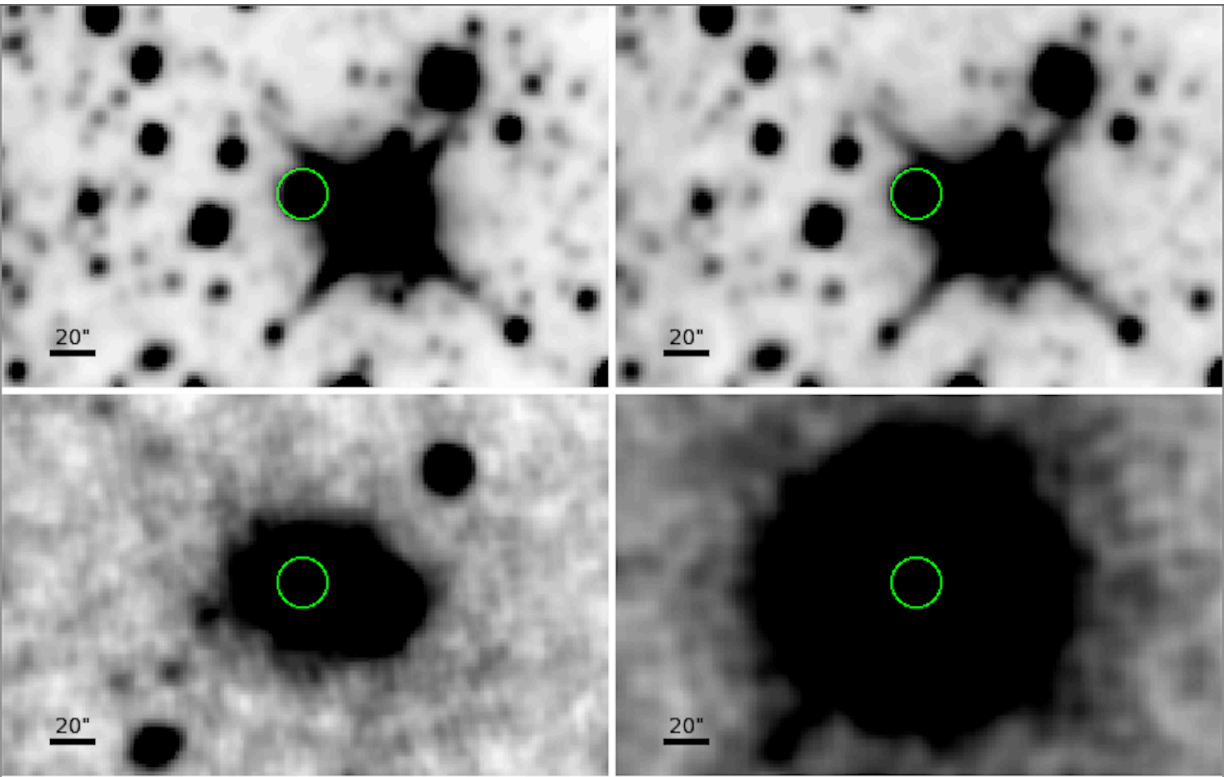


Fig. 3.— WISE band 1 image (top left), WISE band 2 image (top right), WISE band 3 image (bottom left), WISE band 4 image (bottom right). V839 Ara is marked by the green circle on each image. The 81" 'halo' seen in the WISE band 4 image is centered on V839 Ara and is consistent with PSF rings in W4 extending past $\sim 50''$. There is no physical shell

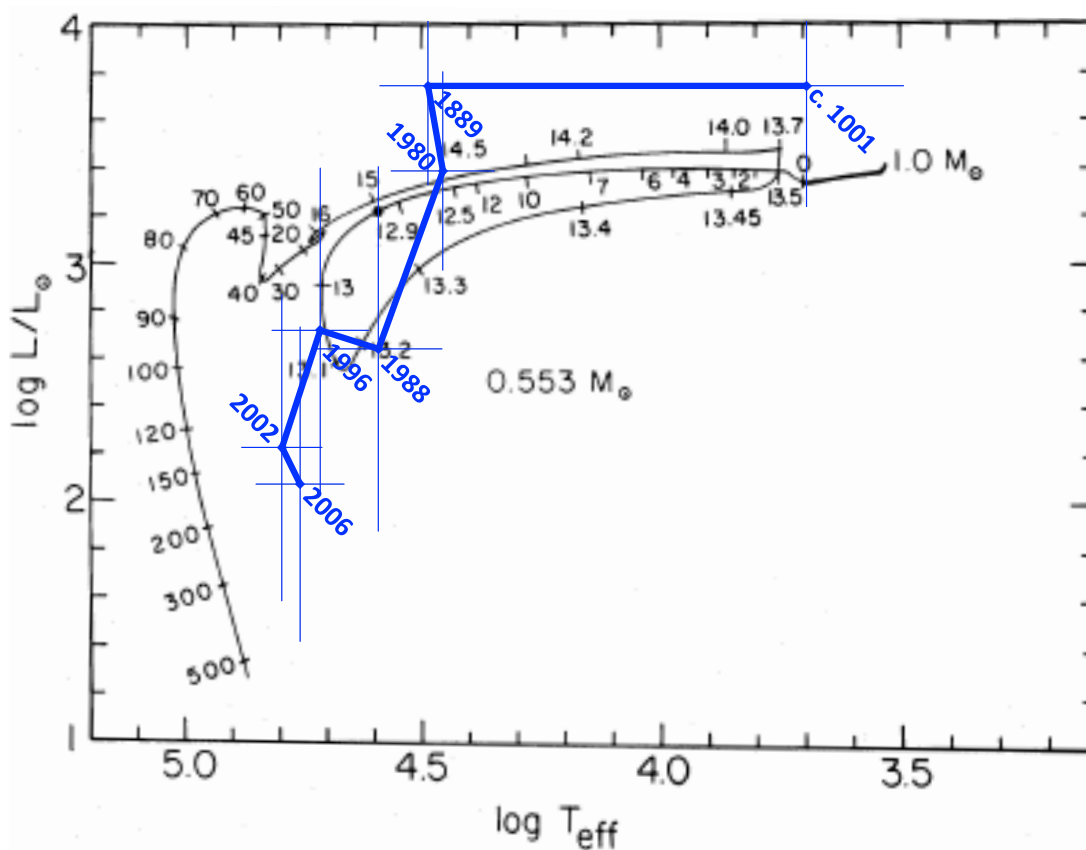


Fig. 4.— The observed versus theoretical evolutionary paths for the Stingray. The theoretical evolutionary path for a $0.553 M_{\odot}$ star is shown as a black curve with tick marks showing the time since the start of the post-AGB phase in units of thousands of years, as copied from Figure 4 of Schönberner (1983). The important points from this are that it takes around 13,000 years from the time of the shell ejection until the star has heated up to 50,000 K, that the time scale for the pulses is from centuries to millennia, and that the range of luminosity is just 0.8 in the logarithm. The observed evolutionary path for the Stingray (the thick blue line with points labeled by the year) is taken from Table 3. The placement of the point for 1001 AD is an approximation of its position when the shell was ejected, with the point being that the observed time scale from shell ejection to the thermal pulse is one order-of-magnitude smaller than theory allows (at least for a non-massive star). The points for 1889 and 1980 can move up-or-down somewhat due to uncertainty in the distance to the Stingray, but the two points move together, so we are left with a vertical segment in the real evolution that does not readily match any model prediction. The last four points (1988-2006) show a path that does not match any model predictions.